Lab on a Chip

ROYAL SOCIETY OF CHEMISTRY

PAPER

View Article Online
View Journal | View Issue

Cite this: *Lab Chip*, 2021, **21**, 1549

A polymer index-matched to water enables diverse applications in fluorescence microscopy†

Xiaofei Han, ‡*[ab] Yijun Su,‡*[ac] Hamilton White, ‡*[de] Kate M. O'Neill, [fg] Nicole Y. Morgan,[h] Ryan Christensen,[a] Deepika Potarazu,[a] Harshad D. Vishwasrao,[c] Stephen Xu,[a] Yilun Sun,[i] Shar-yin Huang,[i] Mark W. Moyle,[j] Qionghai Dai,[b] Yves Pommier,[i] Edward Giniger,[f] Dirk R. Albrecht, ‡[dk] Roland Probst ‡[l] and Hari Shroff‡[acm]

Received 6th December 2020,
Accepted 21st February 2021

DOI: 10.1039/d0lc01233e

rsc.li/loc

We demonstrate diffraction-limited and super-resolution imaging through thick layers (tens-hundreds of microns) of BIO-133, a biocompatible, UV-curable, commercially available polymer with a refractive index (RI) matched to water. We show that cells can be directly grown on BIO-133 substrates without the need for surface passivation and use this capability to perform extended time-lapse volumetric imaging of cellular dynamics 1) at isotropic resolution using dual-view light-sheet microscopy, and 2) at super-resolution using instant structured illumination microscopy. BIO-133 also enables immobilization of 1) *Drosophila* tissue, allowing us to track membrane puncta in pioneer neurons, and 2) *Caenorhabditis elegans*, which allows us to image and inspect fine neural structure and to track pan-neuronal calcium activity over hundreds of volumes. Finally, BIO-133 is compatible with other microfluidic materials, enabling optical and chemical perturbation of immobilized samples, as we demonstrate by performing drug and optogenetic stimulation on cells and *C. elegans*.

Introduction

Fluorescence microscopy spurs biological discovery, especially if imaging is performed at high spatiotemporal resolution and under physiologically relevant conditions. Coupling fluorescence microscopy with strategies for immobilizing or confining samples enables further applications, particularly when studying organisms that move rapidly. For example, the transparency and genetic accessibility[1] of the nematode *C. elegans* has made it an ideal system for studying the growth, morphology and function of individual cells in the context of the whole organism;[2,3] yet imaging the living animal without motion blur usually requires immobilization with chemical,[4,5] steric,[6,7] or microfluidic[8–11] means.

Microfluidic systems provide efficient immobilization and handling[12–18] for studying cellular morphology[19,20] and dynamics,[21] neuronal function,[22–24] behavior,[25–27] and lifespan.[28,29] Hydrogels (either independently[7,30] or in conjunction with microfluidics[31]) have also been demonstrated as highly useful materials with tunable mechanical,[32] diffusive, and optical properties[33] that are well-suited for long-term imaging applications.[7,34,35]

Unfortunately, relatively few attempts have been made to index-match immobilization devices.[36–39] The high refractive index (RI, n) of materials commonly used in microfluidics, such as polydimethylsiloxane (PDMS), causes significant

[a] *Laboratory of High Resolution Optical Imaging, National Institute of Biomedical Imaging and Bioengineering, National Institutes of Health, Bethesda, MD, 20892, USA. E-mail: suy4nih@gmail.com*
[b] *Department of Automation, Tsinghua University, Beijing, 100084, China. E-mail: hxf16@mails.tsinghua.edu.cn*
[c] *Advanced Imaging and Microscopy Resource, National Institutes of Health, Bethesda, MD, 20892, USA*
[d] *Department of Biomedical Engineering, Worcester Polytechnic Institute, 100 Institute Road, Worcester, MA, 01609, USA. E-mail: hawhite@wpi.edu*
[e] *Department of Neurobiology, University of Massachusetts Medical School, Worcester, MA, 01655, USA*
[f] *National Institute of Neurological Disorders and Stroke, National Institutes of Health, Bethesda, MD, 20892, USA*
[g] *Institute for Physical Science and Technology, University of Maryland College Park, College Park, MD, 20742, USA*
[h] *National Institute of Biomedical Imaging and Bioengineering, National Institutes of Health, Bethesda, MD, 20892, USA*
[i] *Developmental Therapeutics Branch and Laboratory of Molecular Pharmacology, Center for Cancer Research, National Institutes of Health, Bethesda, MD, 20892, USA*
[j] *Department of Neuroscience and Department of Cell Biology, Yale University School of Medicine, New Haven, CT, 06536, USA*
[k] *Department of Biology and Biotechnology, Worcester Polytechnic Institute, 100 Institute Road, Worcester, MA, 01609, USA*
[l] *ACUITYnano, Innovation in Biomedical Imaging, North Bethesda, MD, 20850, USA*
[m] *Marine Biological Laboratory Fellows Program, Woods Hole, MA, 02543, USA*
† Electronic supplementary information (ESI) available. See DOI: 10.1039/d0lc01233e
‡ Equal contribution.

optical aberrations[40,41] due to the RI mismatch that occurs at the interface between the polymer (n_{PDMS} ~ 1.41) and an aqueous sample (n_{water} = 1.33). These aberrations severely degrade image focus, resolution, and signal, compromising the performance of immobilization devices by reducing the information content of the resulting data. Hydrogels offer a lower RI (n ranging from 1.34–1.41) depending on thickness and polymerization conditions.[33] Although the RI of these materials is better matched to living samples, even a small mismatch in RI causes a noticeable deterioration in image quality.[42] Image degradation is particularly obvious when using water-dipping lenses designed for imaging living samples, such as those employed in high-resolution light-sheet fluorescence microscopy (LSFM).[43–45]

Here we demonstrate a broadly applicable refractive-index-matched specimen mounting method that introduces negligible aberration when imaging living samples with high-resolution light-sheet microscopy and super-resolution microscopy. We show its utility in combination with microfluidics, enabling applications in high-resolution, volumetric imaging of cells, *Drosophila* tissue, and *C. elegans* adults and larvae. Our method takes advantage of the commercially available UV curable optical polymer BIO-133 (MY Polymers Ltd.) that has a refractive index matched to water (n = 1.333), is non-fluorescent, and is non-toxic. We show that 1) BIO-133 provides a gas permeable, inert, and biocompatible scaffold on which to grow and image tissue culture cells, 2) enables rapid tissue or animal encapsulation, and 3) is compatible with other microfluidic mounting schemes and optical or chemical perturbations.

Results

BIO-133 does not introduce additional optical aberrations

We assessed the optical properties of BIO-133 by using dual-view light-sheet microscopy (diSPIM[43,46]) to image 100 nm yellow-green beads placed under polymer layers of progressively increasing thickness (Fig. 1, methods). In the most common diSPIM implementation, two identical 0.8 numerical aperture (NA) water-dipping objectives mounted above a planar substrate (usually a glass coverslip) alternately illuminate the sample with a light sheet and detect the resulting fluorescence. Since both illumination and detection planes are angled at ~45 degrees with respect to the glass coverslip, imaging through a polymer gel with surface parallel to the coverslip will introduce significant lateral ('x' direction, Fig. 1a) and axial ('z' direction, Fig. 1a) aberrations if the gel's refractive index differs from that of water.

As predicted, we observed this effect when imaging beads embedded under polymers with different RIs (Fig. 1b and c). Under no polymer, images of beads approximate the system point spread function, with measured lateral and axial full width at half maximum (FWHM) 395.9 ± 7.7 nm and 1527.9 ± 119.5 nm (N = 70 beads), respectively. Imaging beads under PDMS caused severe aberrations (Fig. 1c), more than doubling the lateral FWHM under a 25 μm layer (816.8 ± 24.9 nm) with progressive deterioration under thicker polymer layers (Fig. 1b). We also observed aberrations (Fig. 1b and c) under poly(ethylene-glycol) diacrylate (PEG-DA)[7] and fluorinated ethylene polymer (FEP),[47] albeit to lesser extent as the refractive indices of these polymers are closer to water. By contrast, beads imaged under BIO-133 showed negligible visual aberrations or measurable degradation in image quality (Fig. 1b and c, Table S1a†), even under a 150 μm thick film, the largest thickness we tested (lateral FWHM 416.5 ± 8.5 nm). We attribute this result to the refractive index of BIO-133, which we measured to be 1.333. We also verified, under 488 nm, 561 nm, and 639 nm illumination, that BIO-133 introduces negligible autofluorescence (Fig. S1†).

High- and super-resolution imaging of cells through a layer of BIO-133

BIO-133 has permeability to oxygen about 2–3 times greater than PDMS and has water repellent properties (Personal Communication, Ehud Shchori, My Polymers, Ltd.). These material properties are advantageous for maintaining physiologically relevant cell culture conditions. Thus, we

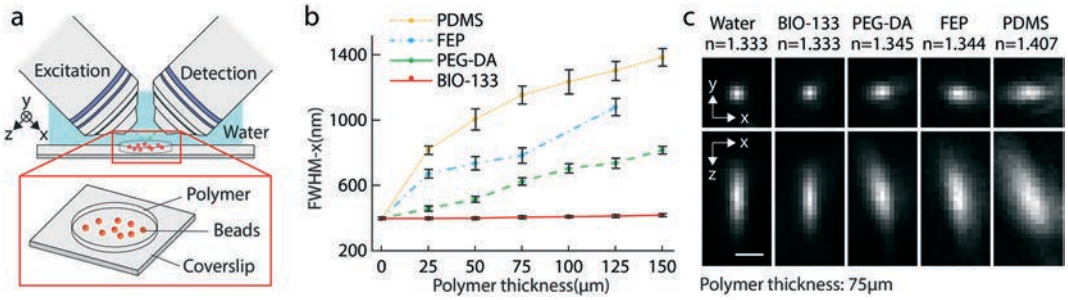

Fig. 1 Diffraction-limited imaging is possible when imaging through BIO-133, unlike other polymers. a) Imaging geometry. A light sheet is used to illuminate the 100 nm yellow-green bead sample, which is embedded under progressively thicker polymer. Illumination and detection occur through 0.8 NA water-dipping objectives. b) Full width at half maximum (FWHM) in the 'x' direction under different thicknesses of polymer. Means and standard deviations are shown. c) Exemplary lateral (top row) and axial (bottom row) images of beads imaged through 75 μm of polymer, demonstrating that BIO-133 provides diffraction-limited performance whilst the other polymers do not. Single images, rather than maximum intensity projections, are shown. The refractive index of each polymer as measured with a refractometer is also indicated (average value from 3 independent trials). Scale bar: 1 μm. See also Table S1a.†

investigated whether BIO-133 could provide an inert and biocompatible scaffold for single cell imaging (Table S2a†). After a curing and leaching treatment (methods), U2OS cells seeded on a 50 μm layer of BIO-133 adhered and displayed similar morphology and growth rate to cells grown on glass coverslips (Fig. 2a and S2†). Similar results were obtained using HCT-116 (human colon carcinoma) cells that express endogenous topoisomerase I-GFP, and we also observed similar expression and localization of tagged proteins compared to cells cultured on glass coverslips (Fig. S2 and S3†).

To demonstrate that transfected cells seeded directly on BIO-133 could be imaged at high spatiotemporal resolution, we created BIO-133 substrates on PDMS supports (Fig. S4†) and imaged cells expressing mEmerald-Tomm20, a fluorescent marker of the outer mitochondrial membrane, through a 50 μm thick BIO-133 layer using diSPIM (Fig. 2b and c). The jointly registered and deconvolved data acquired from two views displayed isotropic spatial resolution (Fig. 2c and d), allowing us to clearly visualize individual mitochondria and their dynamics (Video S1†), including mitochondrial fusion and fission (Fig. 2d). We also used BIO-133 in conjunction with diSPIM to construct a simple gravity-driven flow cytometry setup, obtaining clear images of DAPI stained nuclei as they flowed through the chamber (Fig. S5 and S6, Video S2†).

Next, we sought to image subcellular targets at spatial resolution beyond the diffraction limit, so we turned to instant structured illumination microscopy (iSIM),[48] which enables high-speed super-resolution imaging. We again seeded U2OS cells expressing mEmerald-Tomm20 on a 50 μm BIO-133 film, this time imaging them with iSIM using a water dipping lens in an inverted geometry (Fig. 2e). Again, BIO-133 enabled imaging with minimal aberration (Fig. S7†), enabling us to visualize the internal mitochondrial space absent Tomm20 (Fig. 2f and g, Video S3†). We also visualized LAMP-1-GFP-stained lysosome dynamics in wild type HCT-116 cells grown on another BIO-133 film of 50 μm thickness (Fig. S8, Video S4†). As a third example, we grew multiple layers of HCT-116 cells on BIO-133, and immunostained the cells for lamin A/C, Tomm20, and actin (Fig. 2h), obtaining clear images of these structures through the volume of the sample (Fig. 2i and S7, Video S5†). Quantitative assessment of spatial resolution on biological structures and beads confirmed our visual impression that BIO-133 enables super-resolution imaging with minimal aberration, in contrast to other materials including agarose and PDMS (Fig. S7, Table

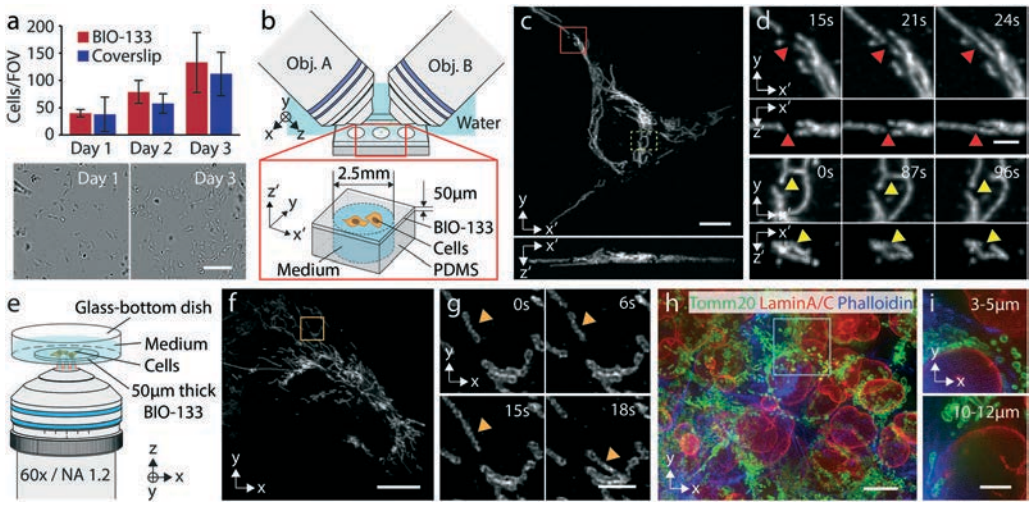

Fig. 2 BIO-133 provides an inert and biocompatible scaffold on which to grow and image cells. a) U2OS growth on BIO-133 is similar to growth on glass coverslips. Top: Quantifying cell growth on 50 μm thick BIO-133 layer *vs.* glass coverslip. Means and standard deviations from 3 fields of view (10× magnification, ~800 μm × 800 μm field of view) are shown over 3 days. Bottom: Example fields of view from day 1 and day 3, cells on BIO-133 layer. Scale bar: 200 μm. See also Fig. S2 and S3.† b) Schematic of diSPIM imaging geometry. 50 μm film with adherent cells is inverted and imaged in the diSPIM setup. See also Fig. S4.† c) Example maximum intensity projections of deconvolved images of U2OS cells expressing mEmerald-Tomm20 in lateral (top) and axial (bottom) views. Scale bar: 10 μm. d) Higher magnification views of the red and yellow rectangles in c), highlighting examples of mitochondrial fusion (top, red arrowhead) and fission (bottom, yellow arrowhead). 50 volumes were taken with a 3 s inter-volume interval. See also Video S1.† Note that primed coordinates refer to the plane of the BIO-133 layer (x', y) and the direction normal to the BIO-133 layer (z'). Scale bar: 2 μm. e) iSIM imaging geometry. Cells were cultured on 50 μm BIO-133 film, and the film placed in a glass-bottom dish and immersed in cell culture medium. Imaging was performed with a 60×, NA 1.2 water-immersion lens. f) Example deconvolved iSIM maximum intensity projection showing live U2OS cells expressing mEmerald-Tomm20. Scale bar: 10 μm. g) Higher magnification view of orange rectangular region in f). Orange arrowhead marks the same mitochondrion. 25 volumes were acquired with a 3 s inter-volume interval. See also Videos S3 and S4.† Scale bar: 2 μm. A 0.5 pixel median filter was used to denoise images in f) and g) prior to display. h) Multiple layers of HCT-116 cells were grown on 50 μm BIO-133 layer and immunostained against Tomm20 (green), lamin A/C (red), and actin (blue). See also Video S5.† Scale bar: 10 μm. i) Maximum intensity projection over indicated axial range (measured from the bottom of the cell layer) for cyan rectangular region in h). Scale bar: 5 μm. See also Fig. S7 and Table S1b.†

S1b†). We conclude that BIO-133 is compatible with multicolor, super-resolution imaging in live and fixed targets.

BIO-133 enables subcellular imaging, segmentation, and tracking within immobilized living tissue

In addition to monitoring the dynamics of organelles within single cells, we also immobilized and imaged multicellular structures in flies and worms at high spatiotemporal resolution, using diSPIM in conjunction with BIO-133 for sample immobilization (Fig. 3, Table S2b†). The developing *Drosophila* wing has long been a model for axon growth and neuronal pathfinding and differentiation.[49,50] More recently, spinning disk confocal microscopy was used to dissect the role of cytoskeletal organization and dynamics in shaping the morphogenesis and growth of the TSM1 pioneer sensory neuron axon in explanted early-pupal wing imaginal discs.[51,52] In those experiments, phototoxicity and photobleaching limited imaging duration to ~30 volumes, with image volumes acquired every 3 minutes. Wings were sandwiched between two glass coverslips to immobilize the preparation and prevent it from moving during imaging, but this scheme introduces unacceptable aberrations if imaging with the less phototoxic diSPIM. Instead, we immobilized wings with a thin layer of BIO-133 (Fig. 3a and S9†), which enabled sustained volumetric imaging with diSPIM. We acquired 360 single-view volumes (5 s inter-volume interval, spanning 30 minutes) of tdTomato-CD4 expressed in TSM1

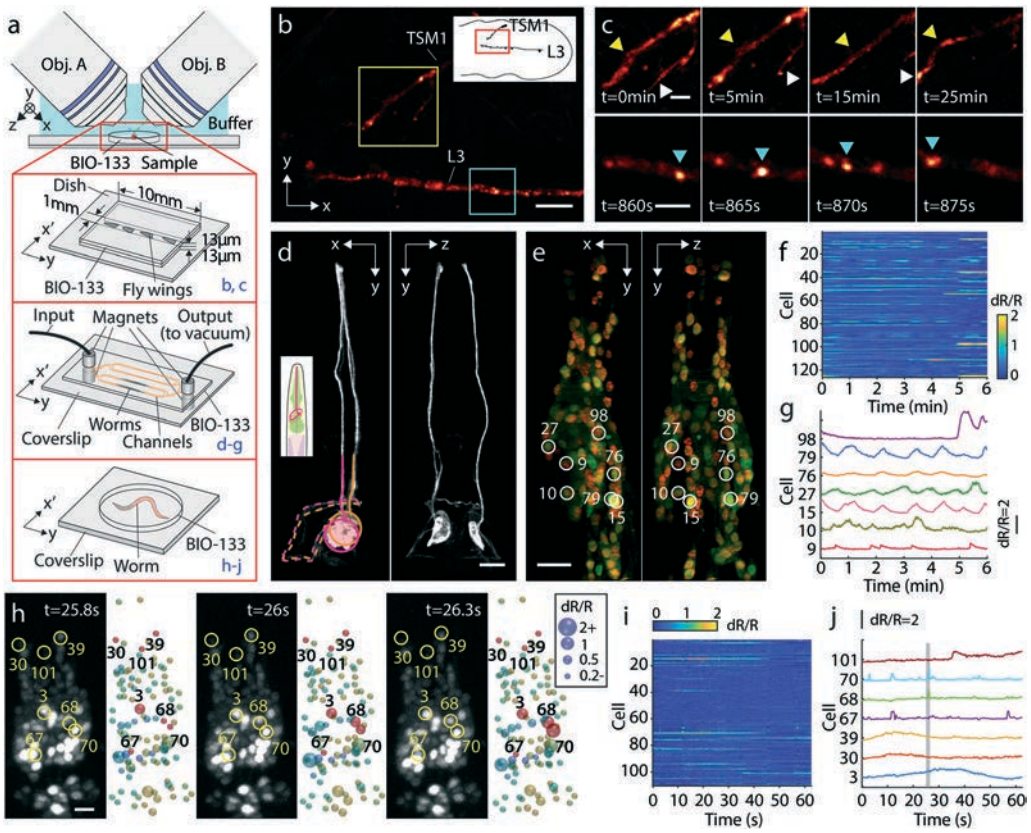

Fig. 3 Live imaging of BIO-133 encapsulated fly wings and *C. elegans*. a) Experimental schematic. Top: A thin layer of BIO-133 membrane covers excised fly wings, immobilizing them so that axon dynamics can be recorded at high resolution over an extended period. Middle: A simple microfluidic device is used to trap adult worms for structural and functional imaging of the nervous system. Bottom: Worms can also be encapsulated in a gelled droplet of BIO-133. See also Fig. S9 and S11.† b) Deconvolved, single-view maximum intensity projection of a fly wing with TdTomato-labelled CD4 showing the axons of two neurons (upper: TSM1; lower: L3) shortly before fasciculation in the developing *Drosophila melanogaster* wing disc. Scale bar: 10 μm. 360 volumes were taken with 5 s inter-volume intervals. (30 min in total, see also Video S6†). c) Magnified regions of TSM1 and L3 axons, corresponding to yellow and blue rectangles in b), highlighting morphological changes and apparent motion of CD4 puncta. Scale bars: 4 μm. d) Isotropic, high-resolution imaging of GFP-labeled axons and dendrites in anesthetized adult *C. elegans*, as shown by orthogonal, jointly deconvolved diSPIM maximum intensity projections. Cell bodies are circled and axons entering the nerve ring region are overlaid with dotted lines. Scale bar: 10 μm. e) Calcium imaging of adult worm (red channel: TagRFP, green channel: GCaMP6s; both labels targeted to nuclei), 2 views imaged at 1.25 Hz volumetric rate. Joint deconvolution diSPIM results are shown; red and green channels were simultaneously collected and colors are overlaid in display. Scale bar: 10 μm. See also Video S7.† f) d*R*/*R* traces for all 126 tracked nuclei. g) d*R*/*R* traces for selected individual neurons. Note correspondence with numbered neurons and marked neurons in e). h) Calcium imaging of larval worm with higher temporal resolution (4 Hz volumetric rate), single-view results are shown. GCaMP channel and associated segmented d*R*/*R* signal are indicated for 3 successive time points. Scale bar: 5 μm. See also Video S8.† i) d*R*/*R* traces for all 110 nuclei segmented and tracked in h). j) Traces for selected individual neurons. Note correspondence with numbered neurons and marked neurons in h).

and the neighboring L3 neuron, marking neuronal membranes (Fig. 3b). In addition to observing slower remodeling of the TSM1 growth cone (Fig. 3c, top) our imaging rate also enabled us to capture rapid movement of membrane-labeled puncta that appeared to traffic along the L3 axon shaft (Fig. 3c, bottom, Video S6†). Puncta were also evident in comparative spinning disk confocal datasets (Fig. S10†).

In another example, we used soft lithography techniques[53] to cast BIO-133 into microfluidic devices suitable for trapping *C. elegans* (Fig. S11†). Introducing adult worms into the channels *via* suction (Fig. 3a), we imaged fine structures

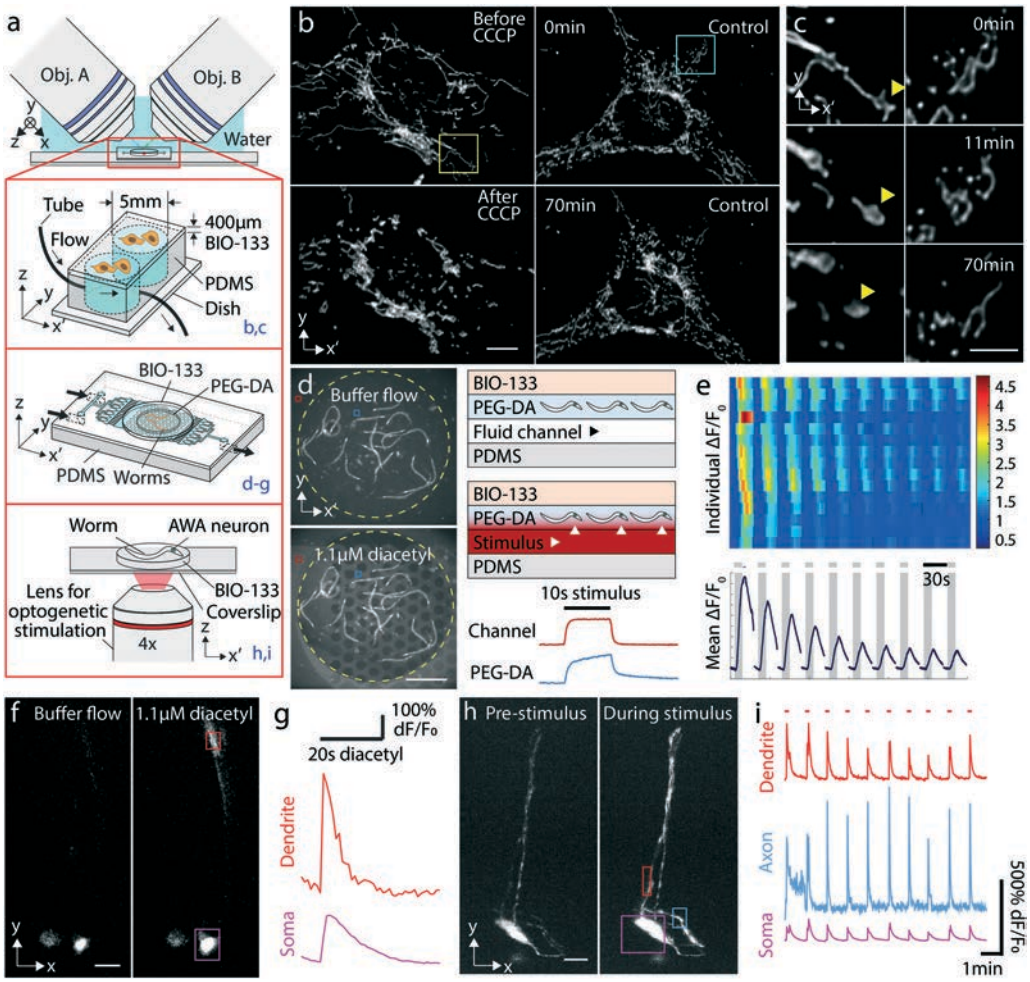

Fig. 4 BIO-133 is compatible with chemical and optical perturbations. a) Experimental schematic for perturbations. Cells grown on BIO-133 were placed on PDMS wells and were either perturbed by flowing 0.05 mM CCCP or left as controls (top higher magnification view). Alternatively, worms were embedded in PEG-DA bonded to a PDMS flow chip and imaged through a layer of BIO-133 (middle higher magnification view) to examine response to chemical stimulation; or embedded in BIO-133, repetitively stimulated with red light from lower, 4× objective and imaged using upper diSPIM objectives (bottom higher magnification view). See also Fig. S12–S14.† b) Example cells with (left column) and without (right column) CCCP treatment at early (top, 0 min) and late (bottom, 70 min) time points. CCCP was added at 10 minutes. Maximum intensity projections of deconvolved diSPIM data are shown. Scale bar: 10 µm. See also Video S9.† c) Higher magnification views of yellow (left column) and blue (right column) regions in b). Yellow arrowhead shows CCCP-induced morphological change of mitochondrion. Scale bar: 5 µm. d) Example images of worms expressing GCaMP immobilized in PEG-DA disk with (bottom) and without (top) 1.1 µM diacetyl. Fluorescein added to stimulus highlights the rapid addition/removal of chemical. Scale bar: 500 µm. Right schematics show layered structure of assembly, including direction of flow and diffusion (arrowheads) into PEG-DA layer. Line plots show intensity of fluorescein over time in channel (red) and PEG-DA (blue) layers. e) Top: d*F*/*F* heatmaps derived from widefield microscopy measurements from 15 animals (rows) in response to 10 repeated stimulus pulses (once per minute). Bottom: responses averaged over all animals show neural adaptation. f) Single-view diSPIM images recorded from a single animal, showing subcellular response in AWA neuron to 1.1 µM diacetyl compared to control (buffer flow) conditions. Contrast has been adjusted to better highlight the response from different cell regions. Scale bar: 10 µm. See also Video S10.† g) Graphs show average intensity from boxed regions in f) highlighting fluorescence intensity changes in soma and dendrite. h) Worms expressing Chrimson and GCaMP are repetitively stimulated with red light and imaged using upper diSPIM objectives. Maximum intensity projection of GCaMP fluorescence from single-view diSPIM recordings are shown before (left) and after (right) optogenetic stimulation. Scale bar: 10 µm. See also Video S11.† i) d*F*/*F* traces for dendrite, axon, and soma, corresponding to boxed regions in h).

(Fig. 3d) and functional activity (Fig. 3e–j) in living animals at isotropic resolution. Animals were sufficiently immobile that we could serially acquire and fuse the two diSPIM views[54] to obtain reconstructions free of motion blur. In strains expressing GFP sparsely targeted to a few neurons, we resolved axons and dendrites (likely from amphid neurons, Fig. 3d) within anesthetized *C. elegans*. When imaging the genetically encoded calcium indicator GCaMP6s[55] and mCherry targeted pan-neuronally[56] in immobilized adult animals without anesthetic, our volume imaging rate of 1.25 Hz (simultaneous acquisition of red and green channels) enabled us to segment and track 126 nuclei in the animal head (Fig. 3e and f, Video S7†), permitting inspection of spontaneously active nuclei (Fig. 3f and g) over our 450 volume (6 minute) experiment. Intriguingly, we observed a pair of nuclei (#79 and #15, Fig. 3e and g) that exhibited in-phase, rhythmic activity with slow (45–80 s) period (Video S7†), as well as nuclei showing out-of-phase activity with respect to this pair (#27). In another experiment, we simply embedded *C. elegans* larvae expressing the same pan-nuclear GCaMP6s marker in a cured disk of BIO-133 (Fig. 3a), recording volumes from one side to obtain volumes at 4 Hz, for 250 volumes. Despite the poorer axial resolution of single-sided imaging, and the smaller size of the larval nuclei, we were able to again segment and track 110 nuclei in the head of the animal, identifying calcium transients in spontaneously active nuclei with a time resolution of 0.25 s (-Fig. 3h–j, Video S8†).

The droplet-based design also enabled easy recovery of animals post-imaging. 26/28 animals were recovered even ~12 hours after embedding, confirming our suspicion that cured BIO-133 is inert, gas permeable, water repellant, and does not obviously affect animal viability (the remaining two animals died within the BIO-133 capsule due to internal hatching of embryos within the animals). The water repellency of BIO-133 likely contributes to retaining the animal's intrinsic hydration and thus viability during encapsulation. The ease at which *C. elegans* can be immobilized and imaged at high spatiotemporal resolution suggests useful synergy with multicolor strategies that permit unambiguous neural identification.[23]

BIO-133 is compatible with chemical and optogenetic perturbations

The ability to specifically perturb and subsequently follow biological processes by observing morphological or functional changes is valuable in dissecting biological processes.

We conducted several studies to show that BIO-133-mounted samples are compatible with such perturbations (Fig. 4). First, we conducted a simple drug assay by modifying our BIO-133/PDMS cellular scaffolds (Fig. 2b and S12†) so that U2OS cells could be exposed (Fig. 4a) to carbonyl cyanide *m*-chlorophenyl hydrazine (CCCP), an inhibitor of oxidative phosphorylation. Because we could clearly observe cells through the BIO-133 layer using diSPIM, we observed that, compared to control cells in a neighboring well (Fig. 4a–c), within minutes of exposure the treated cells showed mitochondrial fragmentation, eventually exhibiting major disruption to the mitochondrial network (Fig. 4b and c, Video S9†).

Chemically stimulating animals directly embedded in BIO-133 is difficult, since BIO-133 is not permeable to aqueous solutions. One solution is to introduce chemicals *via* microfluidic channels (such as those shown in Fig. 3d–g). Alternatively, we explored using PEG-DA for immobilization and aqueous permeability, above a microfluidic layer for stimulus introduction and control, and beneath a BIO-133 layer to enclose the fluidic path. Using a thin PEG-DA disk allows easy transfer of different embedded organisms on the same imaging setup, and repeated imaging of the same animals over many hours if desired. We constructed a hybrid multi-material device composed of a PDMS microfluidic base bonded to a BIO-133 upper membrane that sealed in a small PEG-DA disk containing tens of embedded nematodes[7] (Fig. S13† and 4a). Chemicals applied *via* flow channels diffuse into the PEG-DA disk, evoking neural responses that can be imaged through the BIO-133 viewing layer with widefield microscopy or diSPIM (Fig. 4d–g, methods). We embedded 15 animals expressing GCaMP2.2b in AWA chemosensory neurons[57] in a PEG-DA disk and applied 1.1 μM diacetyl pulses, which directly activate these neurons *via* the ODR-10 chemoreceptor.[57,58] Using widefield microscopy, we recorded robust calcium transients from all animals and observed a characteristic sensory adaptation to repeated stimulation (Fig. 4e). The initiation of sensory neural responses varied slightly due to diffusion of diacetyl stimulus through the PEG-DA disk to animals embedded in different planes (Fig. S14†). Next, we examined individual neuron responses by using the same apparatus with diSPIM (Fig. 4f and g, Video S10†). Our imaging provided sufficient spatial resolution to distinguish subcellular responses, observing faster on and off dynamics of fluorescent transients in the dendrites than in the soma.[59]

Other stimulation modalities (such as light, temperature, and mechanical vibration) are directly transmissible through BIO-133, and these can be applied directly to cells and organisms embedded in the polymer in a simpler preparation. Optogenetic neural activation is a particularly advantageous tool, allowing remote light-induced activation or suppression of neurons. We embedded nematodes expressing the red light activated cation channel Chrimson[60] and GCaMP2.2b[7] directly in BIO-133 disks and monitored calcium readout with diSPIM during repeated red light stimulation pulses (Fig. 4a, h and i, Video S11†). We observed increases in fluorescence after each stimulus (Fig. 4h), and again could clearly localize such transients to subcellular areas including soma, dendrite, and axon (Fig. 4i).

Discussion

BIO-133 is commercially available, rapidly curing, gas permeable, inert, water repellent, and biocompatible. The

mechanical properties of BIO-133 are similar to PDMS (Table S3†). BIO-133 is not autofluorescent under visible illumination and does not introduce additional aberration when imaging with water-dipping or water-immersion objective lenses designed for aqueous specimens. These characteristics make it well-suited to microfluidic experiments under physiological conditions, particularly with the many LSFM systems that use such lenses. We suspect that capillary mounting,[47] often used for mounting zebrafish in LSFM, could be improved if BIO-133 were used instead of the FEP material commonly used in this application. Our finding that cells can be directly grown on BIO-133 without additional surface treatment may prove useful in non-standard LSFM geometries that previously employed RI-matched materials with passivated surfaces,[45] or in ultra-high-throughput light-sheet imaging.[61,62]

We also found that BIO-133 does not noticeably degrade imaging performed in more traditional inverted microscope geometries, including in super-resolution imaging. This capability suggests that using BIO-133 could improve imaging in studies of cell morphology, mechanics, migration, and motility, *e.g.*, when using micropillars[20,63] or in traction force microscopy.[64]

We bonded BIO-133 to glass and PDMS with silicone-based adhesive tape, or reversibly to glass *via* van der Waals forces. The elastic modulus of cured BIO-133 (5 MPa) is similar to that of PDMS (3 MPa). Thus, similar to PDMS,[65] BIO-133 conforms to minor imperfections in glass and bonds to it by weak van der Waal forces, creating a reversible bond and a watertight seal. We suspect further tuning of adhesive, optical and mechanical properties of this intriguing polymer is possible but will depend on knowing the chemical formula, which is currently proprietary.

Materials and methods

Sample preparation

U2OS, wild type (WT) HCT-116, and HCT-116 TOP1-GFP cell culture. U2OS (ATCC, HTB-96), WT HCT-116 (ATCC, CCL-247), and HCT-116 TOP1-GFP (see below) cells were cultured in DMEM (Lonza, 12-604F) media with 10% fetal bovine serum at 37 °C and 5% CO_2.

To tag the genomic topoisomerase I (TOP1) in WT HCT-116 cells, sequence CCTCACTTGCCCTCGTGCCT targeting a CRISPR site 77 nt after the stop codon of TOP1 was cloned into pX330. Homology arms (of ~1 kb) upstream and downstream of the target site were cloned to flank a blasticidin-resistance gene, where the upstream homology arm was modified to replace the stop codon with a GFP domain connected to the protein-coding region of the last exon of TOP1 *via* a short poly-lysine linker. Both constructs were co-transfected into WT-HCT116 cell, followed by selection with 5 μg mL^{-1} of blasticidin 48 hours post transfection. GFP-positive cells were further selected by FACS.

Transfection of cells. Cells were cultured to 50% confluency and transfected using xTreme Gene HP DNA transfection reagent (Sigma, 6366236001). The transfection mixture contained 100 μL 1X PBS, 2 μL transfection reagent, and 200–1000 ng plasmid DNA. Cells were imaged 24–48 hours after transfection.

***C. elegans* samples.** Nematode strains were grown on NGM plates seeded with OP50 bacteria. *C. elegans* imaged as young adults were synchronized by picking L4 stage worms 24 hours prior to the experiment and transferring them to seeded plates, and *C. elegans* imaged as larvae were directly picked from plates. Strain DCR6268 (*olaEx3632*[*pttx-3b::SL2::Pleckstrin homology domain::GFP::unc-54 3′UTR + pelt-7::mCh::NLS::unc-54 3′UTR*]) was used for imaging axons and dendrites (Fig. 3d). *olaEx3632* was made by injecting plasmid DACR2285 (*pttx-3b*::*SL2*::*Pleckstrin homology domain*::*GFP*::*unc-54 3′UTR*) at 25 ng uL^{-1} and DACR2436 (*pelt-7*::*mCh*::*NLS*::*unc-54 3′UTR*) at 10 ng μL^{-1}. Strain AML32 (ref. 56) (*wtfIs5* [*rab-3p::NLS::GCaMP6s + rab-3p::NLS::tagRFP*]) was used for pan-nuclear neuronal calcium imaging (Fig. 3e–j); strain NZ1091(*kyIs587* [*gpa-6p::GCaMP2.2b*; *unc-122p::dsRed*]; *kyIs5662* [*odr-7p::Chrimson:SL2:mCherry*; *elt-2p::mCherry*][7]) was used for chemical (Fig. 4d–g) and optogenetic stimulation (Fig. 4h and i). For optogenetic stimulation, L4 stage animals were transferred to agar plates seeded with 62.5 μM all trans-retinal (ATR, Sigma Aldrich, R2500) for over 12 hours.

Drosophila samples. *Drosophila* stocks were obtained from the Bloomington *Drosophila* Stock Center: *neur-GAL4* (BL6393) and *UAS-CD4-td-Tomato* (BL35837). White prepupae were selected and aged for 13–14 h at 18 °C followed by 1 h at 25 °C (equivalent to 7.5–8 h at 25 °C). These aged pupae were dissected in fresh culture media (CM; Schneider's *Drosophila* media + 10% fetal bovine serum, both from Life Technologies), and wing discs were isolated from the aged pupae and stored in fresh CM prior to mounting with BIO-133.

Characterizing the optical properties of polymers

Characterization of aberrations by visualizing fluorescent beads through different polymer layers. 100 nm diameter yellow-green fluorescent beads (Invitrogen, F8803, 1 : 10 000 dilution in water) were coated on #1.5 coverslips (24 mm × 50 mm, VWR, 48393-241) coated with 0.1% w/v poly-L-lysine (Sigma, P8920-100ML). For light-sheet microscopy, we placed spacers (Precision Brand, 44910) of variable thickness on one of the coverslips and deposited droplets of BIO-133, 10% PEG-DA (ESIBIO, GS705) or UV-curable PDMS (Shin-Etsu Chemical, KER-4690) on the beads. The droplet was then covered with another coverslip coated with beads and compressed with an iron ring. BIO-133 and PEG-DA hydrogels were crosslinked at 312 nm (Spectroline ENB-280C) for 2 minutes. PDMS was crosslinked at 312 nm for 5 minutes and post-cured at room temperature for one day. Once cured, we separated the two cover glasses and kept the one with polymer/hydrogel on it. For imaging through FEP films of different thickness (CS Hyde, 23-1FEP-24, 25 μm; 23-2FEP-24, 50 μm; 23-3FEP-24, 75 μm; 23-5FEP-24, 125 μm), we

immersed beads in 1 μL water and covered the sample with the FEP film. All bead images were acquired with a symmetric 0.8/0.8 NA diSPIM.[43] For super-resolution microscopy, we made 50 μm layers of BIO-133, 2% agarose, or UV-curable PDMS between two coverslips coated with beads as described above. BIO-133 and PDMS were cured with UV light, and agarose was cured by cooling to room temperature. Bead images were acquired with a 60×/1.2 NA water immersion lens using an instant structured illumination microscope (iSIM[48]).

Measurement of refractive index of polymers. A refractometer (American Optical) was used to measure the refractive index of pure water, BIO-133 film (My Polymer, BIO-133, 25 μm), PDMS film (Shin-Etsu Chemical, KER-4690, 25 μm), FEP film (CS Hyde, 23-1FEP-24, 25 μm), and 10% PEG-DA hydrogel (100 μm). The refractive index for each material was measured 3 times and the average value reported in Fig. 1.

Measurement of BIO-133 autofluorescence. A 50 μm thick BIO-133 film was deposited on a glass bottom dish (MatTek, P35G-1.5-14-C). Images were acquired both on the BIO-133 area and an area without BIO-133, using an instant structured illumination microscope (iSIM[48]) with 40 ms exposure time and 45 mW 488 nm excitation, 70 mW 561 nm excitation, or 90 mW 639 nm excitation (measured with a power meter immediately prior to the objective). Care was taken to ensure the illumination was focused within the BIO-133 film. The two images were subtracted to measure the autofluorescence of BIO-133 relative to glass (Fig. S1†).

Cell growth and imaging using BIO-133 substrates

Fabrication of BIO-133 cell culture wells for diSPIM experiments. BIO-133-sided PDMS substrates with 2.5 mm diameter wells (Fig. S4†) were used for live cell imaging experiments (Fig. 2b–d). To make the BIO-133 bottom, a BIO-133 droplet was positioned on a #1.5 glass coverslip (24 mm × 50 mm, VWR 48393-241) between two 50 μm plastic spacers (Precision Brand, 44910), covered with another coverslip, compressed with a glass slide (Ted Pella, 260386) and cured with a UV lamp (365 nm, Spectroline ENB-280C) for 15 minutes. After curing, the BIO-133 film was peeled off and exposed to UV light for another 2 hours in 70% ethanol. To make the PDMS well, 15 mL PDMS (Dow Inc. Sylgard 184) was poured into a 10 cm plastic dish (Kord-Valmark, 2910) and cured for 2 hours at 80 °C to obtain a 2 mm thick PDMS slab. We punched 2.5 mm diameter matching holes on the PDMS slab and a piece of double-sided tape (Adhesives Research, ARCare 90880) using a 2.5 mm diameter circular punch (Acuderm Inc., P2550). The PDMS slab and the tape were then cut into smaller pieces (~5 mm on a side) with a razor blade (Sparco, 01485). BIO-133 membranes, PDMS chunks and double-sided tape were further disinfected in 70% ethanol for 2 hours. After disinfection, the BIO-133 membrane was adhered to PDMS using the adhesive tape, so that the matching holes became wells for cell culture. After seeding and growing cells in wells, the assembly was flipped over for diSPIM imaging.

Quantification of cell growth. Cured and leached 50 μm thick BIO-133 films were deposited on glass bottom dishes (MatTek, P35G-1.5-14-C). Similar aliquots of U2OS (or HCT 116 TOP1-GFP) cells were seeded onto BIO-133 films or on another glass bottom dish without BIO-133 (MatTek, P35G-1.5-14-C). Dishes seeded with cells were maintained between imaging experiments in an incubator at 37 °C, 5% CO_2. On each dish, a small area was selected and imaged using a widefield microscope equipped with a 10×/0.25 NA objective lens each day, for three days. Cells numbers were estimated from images with the cell counter ImageJ plugin (https://imagej.nih.gov/ij/plugins/cell-counter.html). Each experiment was repeated three times. Raw images were divided by Gaussian-blurred versions of themselves (sigma = 5 pixels) to flat-field images prior to display (Fig. 2a and S2†).

Live cell imaging through BIO-133 with diSPIM. U2OS cells were cultured and transfected with 100–200 ng of mEmerald-Tomm20 plasmid (Addgene, 54281) directly on the BIO-133 bottomed well plate. The well plate was inverted and immersed in live cell imaging solution (Invitrogen, A14291DJ). Cells were imaged with a symmetric 0.8/0.8 NA diSPIM, through the BIO-133 layer. 50 volumes were acquired with 3 s intervals between dual-view volumes. Dual-view data were jointly deconvolved with ImageJ plugin diSPIM Fusion,[54] and were drift- (with ImageJ plugin Correct 3D Drift (https://imagej.net/Correct_3D_Drift) and bleach-corrected (with ImageJ function Bleach Correction (https://imagej.net/Bleach_Correction, exponential fitting method) prior to display.

Super-resolution imaging through BIO-133 with iSIM. U2OS or WT HCT-116 cells were cultured and transfected with mEmerald-Tomm20 or LAMP1-EGFP (Taraska Lab, NHLBI) on a 50 μm thick BIO-133 film. The BIO-133 film was cured on a glass bottom dish (MatTek, P35G-1.5-14-C). A 60×, NA = 1.2 water objective (Olympus, PSF grade), correction collar adjusted to 0.17, was used to image the cells through the glass and BIO-133 film using our home built iSIM system[48] and 488 nm excitation. Volumes were acquired every 3 s for U2OS cells expressing mEmerald-Tomm20 and every 7 s for WT HCT-116 cells expressing LAMP1-EGFP. We used an exposure time of 80 ms, and a *z*-step of 0.25 μm for U2OS cells and 0.5 μm for WT HCT-116 cells. Live HCT-116 TOP1-GFP cultured on a 50 μm thick BIO-133 film or on a glass bottom dish were imaged to acquire volumes with a step size of 0.5 μm. Raw images were deconvolved with the Richardson–Lucy algorithm for 20 iterations, destriped in Fourier space to remove striping artifacts,[66] and bleach corrected (https://imagej.net/Bleach_Correction). A median filter with kernel size 0.5 pixel was applied to denoise mEmerald-Tomm20 and GFP-LAMP1 images prior to display. Resolution estimation on images was performed with a decorrelation analysis ImageJ plugin.[67]

Immunolabeling and imaging of multilayered WT HCT-116 cells on BIO-133. WT HCT-116 cells were cultured on a

50 μm thick BIO-133 film on a glass bottom dish until a thick layer was visible by eye. Cells were fixed with 4% paraformaldehyde (Electron Microscopy Sciences) in 1× PBS for 30 minutes at room temperature (RT). Cells were rinsed 3 times in 1× PBS and permeabilized with 0.1% Triton X-100/PBS (Sigma, 93443) for 15 min at RT. Permeabilized cells were rinsed 3 times with 1× PBS and incubated in 1× PBS with primary antibody Rabbit-α-Tomm20 (Abcam, ab186735) and Mouse-α-laminA/C (Abcam, ab244577) at a concentration of 1 : 100 for 1 hour at RT. After primary antibody staining, cells were washed in 1× PBS for 5 min, three times. Cells were stained in 1× PBS with secondary antibody Donkey-α-Rabbit Alexa Fluor 488 (Jackson Immuno Research, 711-547-003), Donkey-α-Mouse JF549 (Novusbio, NBP1-75119JF549) and Alexa Fluor 647 Phalloidin (Thermo Fisher, A22287) at a concentration of 1 : 100 for 1 hour at RT. Cells were washed in 0.1% Triton X-100/PBS for 5 min, three times. In each spectral channel, 46 slices were acquired on iSIM with an exposure time of 100 ms and a *z*-step of 0.5 μm. Raw images were deconvolved with the Richardson–Lucy algorithm for 20 iterations and destriped in Fourier space to remove striping artifacts.[66] The 633 nm channel (Alexa Fluor 647 Phalloidin) was bleach corrected (https://imagej.net/Bleach_Correction) across the *z* stack to compensate for decreased signal further into the stack.

Flow cytometry preparation. Sample handling channels, 1 mm wide and 70 μm high, were formed by pouring 20 mL PDMS (Dow Corning, Sylgard 184) on a positive mold made of packaging tape (Duck Brand) cut to the desired dimensions with a craft cutter (Silhouette Cameo) and stuck in a 10 cm Petri dish. A thin PDMS membrane (~0.5 mm) was air plasma (Harrick Plasma, PDC-32G (115 V)) bonded to the channel surface. Holes at the endpoints of the channel were created by punching the PDMS membrane with a 1 mm diameter circular punch (Acuderm Inc., P150) after plasma treatment. A 400 μm wide (142 μm height) imaging channel was cut directly from double-sided silicon-based adhesive tape (Adhesives Research, ARCare 90880) with a craft cutter and stuck to the PDMS device, thus creating a connection between the two sample handling channels in the lower layer. A thin BIO-133 membrane (50 μm) was placed on top of the tape to seal the channel. Two thick PDMS pieces with holes (6 mm and 2 mm diameter) were cut and air plasma bonded to the device to provide fluidic access. When imaging, cells were added to the 6 mm diameter reservoir, and output tubing (Dow Corning, 508-004) was connected to the 2 mm hole. Flow speed was adjusted by changing the height of the output tubing. See also Fig. S5.†

Flow cytometry imaging of fixed, DAPI-stained U2OS cells. U2OS cells were fixed in 4% paraformaldehyde/PBS and subsequently stained with DAPI in 0.1% Triton X-100/PBS (Sigma, 93443). The flow device was mounted on a 10 cm Petri dish for imaging with diSPIM. Fixed cells were added to the input port, producing steady flow through the channel after several minutes. 1000 frames of the same image plane were acquired with diSPIM at 50 frames per second under 'fixed sheet mode'.

Live animal/tissue imaging through BIO-133 with diSPIM

Live imaging of BIO-133 embedded *Drosophila* wings. A 13 μm thick BIO-133 film was created and cut into two rectangular pieces (4.5 mm × 10 mm) and a square piece (10 mm × 10 mm). The rectangular pieces were deposited on a 10 cm Petri dish to form a 1 mm wide open-top channel. Early pupal fly wings were deposited into the channel (convex side up) with 20–40 μL culture media, the square BIO-133 piece placed on top to close the channel and additional culture media was carefully added to the dish (Fig. 3a and S9†). Single-view diSPIM imaging was then performed. 360 volumes were acquired with 5 s inter-volume spacing, over 30 minutes. Volumes were deconvolved with MATLAB and bleach corrected with ImageJ (https://imagej.net/Bleach_Correction, exponential fitting method).

Fabrication of microfluidics for *C. elegans* immobilization. Standard soft lithography techniques[68] were used to fabricate an SU-8 (Kayaku Advanced Materials, formerly Microchem Corp.) master mold for sets of four microfluidic funnels for worm confinement as described.[53] To fabricate devices in BIO-133 (MY Polymers Ltd.), we placed two spacers (100 μm, Precision Brand 44910) beside the pattern, poured polymer onto the mold, covered the mold with a glass slide and cured the polymer under a UV lamp (365 nm, Spectroline ENB-280C) for 2 minutes. After curing, we peeled the BIO-133 off the mold, punched inlet and outlet holes with a 1 mm diameter circular punch (Acuderm Inc., P150), and sealed the device to a #1.5 cover glass (24 mm × 50 mm, VWR 48393-241) with double-sided silicone-based adhesive tape (Adhesives Research, ARCare 90880). We cut out an aperture from a 10 cm Petri dish and used UV-curable optical cement (Norland Products Inc., Norland Optical Adhesive NOA 68) to secure the coverslip carrying the microfluidic device over the aperture in the Petri dish. Inlet and outlet tubing (Dow Corning, 508-004) was clamped to the assembly using a pair of hollow magnets (K&J Magnetics, R211-N52) placed above and below the coverslip, as described.[69] Optical cement was again used to secure tubing to the magnets. See also Fig. S11.†

Live imaging of *C. elegans* through BIO-133 chambers. To load worms into the immobilization device, we added a drop of M9 buffer containing worms to the inlet and created vacuum at the outlet using a syringe. Within several minutes (for a 4-channel chip), worms were observed to align in the channels. The Petri dish was then filled with water and worms were imaged with symmetric 0.8/0.8 NA diSPIM. For structural imaging, we added 0.25 mM levamisole to the buffer to stop residual worm motion. For calcium imaging, the outlet was connected to a peristaltic pump (Dolomite Microfluidics, 3200243) which provided negative pressure to immobilize worms without using anesthetics. We simultaneously imaged nuclei structure (TagRFP) and the nuclear-localized calcium response (GCaMP) with 488 nm and 561 nm excitation (Coherent) and image splitting devices on the detection side (Hamamatsu W-VIEW GEMINI), using a

previously described fiber-coupled diSPIM system.[46] Dual-view stacks were acquired every 0.8 s over 500 time points. Dual-color, dual-view images were deconvolved and registered with ImageJ plugin diSPIM Fusion.[54]

Droplet-based immobilization of nematodes prior to imaging, and recovery after imaging. *C. elegans* were directly transferred from agar plates into a drop (~10 μL) of BIO-133 or 10% PEG-DA (ESIBIO GS705) on a #1.5 cover glass (24 mm × 50 mm, VWR, 48393-241). The droplet was positioned between two 100 μm spacers (Precision Brand, 44910), and was compressed by a glass slide followed by 2 minute polymerization under a UV lamp (365 nm, Spectroline ENB-280C). After polymerization, worms were immobilized in the resulting gel disk. The gel disk was then placed in a 10 cm Petri dish or a standard chamber for diSPIM imaging. Single-view stacks were acquired every 0.25 s for 250 time points. After imaging, worms could be released and checked for viability by gently breaking the droplet with forceps. In some experiments, we immersed the disks in M9 buffer for up to 12 hours, finding that live worms could also be recovered after this period.

Tracking nuclei, calcium imaging analysis. TagRFP volumes were imported into Imaris and neurons tracked with Imaris for tracking (https://imaris.oxinst.com/products/imaris-for-tracking) to obtain the center of each neuron at every timepoint. A custom MATLAB script was used to extract the calcium signal. For every neuron, the average intensity of TagRFP channel I_{561} and the intensity of GCaMP channel I_{488} were computed by averaging pixels within a 2 μm (adult) or 1.5 μm (larval) diameter sphere placed around each center position. I_{561} and I_{488} were calculated from dual-view deconvolved images (Fig. 3f and g) or single-view raw data (Fig. 3i and j). The ratio $R = I_{488}/I_{561}$ was used to minimize non-GCaMP fluctuations. Neuronal activity for the datasets in Fig. 3 was reported as $dR/R = (R - R_0)/R_0$, where R_0 is the baseline for an individual neuron defined as its lower 20th percentile intensity value.

Chemical and optical perturbations in BIO-133 based imaging devices

Fabrication of chemical delivery devices for cells. A modified PDMS well plate design (Fig. S12†) was applied to deliver chemical perturbations to cells (Fig. 4a–c). A 400 μm thick BIO-133 film was created using the method described above. 10 mL PDMS was cured in a 10 cm dish, PDMS tubing (Dow Corning, 508-004) was placed on the cured PDMS layer at 8 mm intervals, and another 15 mL PDMS was added to obtain a ~4 mm thick PDMS slab with channels contained inside. Holes crossing the channels were punched at 8 mm intervals using a 5 mm diameter circular punch (Acuderm Inc., P550). A piece of double-sided silicone-based adhesive tape (Adhesives Research, ARCare 90880) was also punched at 8 mm intervals using a 2.5 mm diameter circular punch (Acuderm Inc., P2550). The PDMS slab and the tape were cut into two-well pieces. BIO-133 film, PDMS chunks and double-sided tape were disinfected in 75% ethanol. After disinfection, the BIO-133 membrane was adhered to PDMS *via* the double-sided adhesive tape, so that the matching holes became wells for cell culture. After growing cells, tubing (Scientific Commodities Inc., BB31695-PE/2) was inserted into both sides of the channel for introducing chemical flow and another piece of double-sided tape without holes was used to seal the wells. The assembly was flipped over for diSPIM imaging through the BIO-133 membrane.

Mitochondrial imaging in the presence of CCCP. U2OS cells were cultured in two 5 mm diameter BIO-133 bottomed wells with ports and transfected with 300–400 ng of mEmerald-Tomm20. Before imaging, the wells were filled with live cell imaging solution (Invitrogen, A14291DJ), flipped over and attached to a 10 cm Petri dish with double-sided silicone-based adhesive tape (Adhesives Research, ARCare 90880). For the well containing control cells, tubing was left disconnected from a source. For the well containing cells that experienced chemical perturbation, input tubing was connected to a syringe containing 0.05 mM carbonyl cyanide *m*-chlorophenyl hydrazine (CCCP, Sigma, C2759). The syringe is higher than the output tube so that drug flow was induced by gravity. We used a valve (McMaster-Carr, 7033T21) placed between the input tube and syringe to control the flow. The valve was closed prior to imaging. For each well, two cells were chosen for imaging. A multi-position acquisition was set in the Micro-manager[70] diSPIM plugin[71] to sequentially image the four cells. Volume acquisition time was 3 s, and 90 volumes were acquired for each cell with 60 s intervals between volumes. 10 minutes after the imaging started, the valve was opened and drug flow was induced in ~60 s. Dual-view images were deconvolved with ImageJ plugin diSPIM Fusion,[54] drift corrected (ImageJ plugin Correct 3D Drift, https://imagej.net/Correct_3D_Drift) and bleach corrected (ImageJ function Bleach Correction, https://imagej.net/Bleach_Correction, exponential fitting method).

Encapsulation of *C. elegans* into PEG hydrogels. *C. elegans* were encapsulated into PEG hydrogel disks as described in our prior work.[7] PEG hydrogel precursor solutions were prepared by combining 20% w/v poly(ethylene glycol) diacrylate (PEG-DA, 3350 MW, 94.45% acrylation, ESI BIO) with 0.10% w/v Irgacure 2959 photoinitiator (2-hydroxy-4′-(2-hydroxyethoxy)-2-methylpropiophenone, I2959, BASF) in 1× S-basal buffer (100 mM NaCl, 50 mM KPO_4 buffer, pH 6.0). Clean 24 mm × 50 mm glass coverslips (VWR) were rendered permanently hydrophobic by exposure to vapors of (tridecafluoro-1,1,2,2-tetrahydrooctyl) trichlorosilane (Gelest). For covalent attachment of the PEG hydrogel to glass, coverslips (Thermo Scientific) were silanized by coating with 3-(trimethoxysilyl)propyl methacrylate (TMSPMA, Sigma-Aldrich). Both methods of surface modification were applied to 1″ × 3″ glass slides (VWR). A small volume (1.75 μL) of PEG hydrogel solution with photoinitiator was pipetted onto a hydrophobic glass slide flanked by two PDMS spacers whose thickness matched the desired hydrogel thickness of 150 μm. Animals were transferred into the hydrogel solution

by worm pick. A coverslip, TMSPMA treated for making mounted PEG-DA gels, or untreated for making freestanding gels, was placed over the hydrogel droplet and supported by the PDMS spacers. The glass slide/coverslip sandwich was then placed over a UV light source (312 nm, International Biotechnologies, Inc, model UVH, 12 W) and illuminated for two minutes until gelation. Hydrogel disks were immediately transferred to wet agar dishes to keep embedded animals hydrated.

Fabrication of microfluidic devices for chemical stimulation of *C. elegans*. Microfluidic chambers were prepared using poly(dimethyl siloxane) (PDMS; Sylgard 184, Dow Corning) in a ratio of 1 : 10 and poured to a depth of 5 mm on a silicon master positive mold of the microchannels used previously.[72] Once cut free of the master, devices were punched so that two balanced-length inlets and the outlet had 1.5 mm holes going through the thickness of the material, and 1 mm holes punched from the side to allow flexible tubing to be inserted from the sides. The smooth PDMS device surface opposite the microchannels was irreversibly bonded to a glass slide using oxygen plasma (Harrick PDC-32G, 18 W, 45 seconds). A thin PDMS membrane (150 μm) was cut with a 3.5 mm diameter dermal punch and then oxygen plasma bonded to the microfluidic channel surface with the hole in the membrane exposing the micropost array. The hole in the thin PDMS membrane formed a "well" that hydrogel disks could be gently placed in with forceps. A thin BIO-133 membrane (75–80 μm) was prepared by gelation of BIO-133 liquid polymer between two glass slides rendered permanently hydrophobic as described above. Two layers of clear cellophane tape (height of ~80 μm) formed the standoffs that determined final membrane height. After degassing the microfluidic device in a vacuum chamber for approximately 45 minutes, the device was removed from the desiccator, connected to tubing, and flushed with S. basal buffer before use to remove any air bubbles. Hydrogel disks could be interchanged between the well formed by the PDMS above the micropost array easily using forceps and then the system sealed for microfluidic flow using the thin BIO-133 membrane described above. See also Fig. S13.†

Preparation of chemosensory stimulus. For both wide-field and diSPIM assays, diacetyl (2,3-butanedione, Sigma) was diluted to 1.1 μM in 1× S. basal (10^{-7} dilution). 1 μL of 1 mg mL^{-1} fluorescein solution was added to 40 mL of diacetyl solution to visualize stimulus delivery.

Wide-field imaging with chemical stimulation. For wide-field, single plane imaging of multiple *C. elegans* at once,[57] the microfluidic chamber, valves, tubing and reservoirs were prepared as above and placed on a Zeiss AxioObserver epifluorescence microscope with a 5×, 0.25 NA objective, EGFP filter set, and Hamamatsu Orca-Flash 4 sCMOS camera. Micromanager scripts[73] automatically synchronized capture of ten 30 s trials recording at 10 fps with 10 ms excitation pulses and 10 s chemical stimulation. NeuroTracker software[72] analyzed the wide-field neural imaging data, from which background-corrected fluorescence changes were calculated in MATLAB as $\Delta F/F_0$, where F_0 is baseline neural fluorescence during the four seconds prior to stimulation. Data for multiple individual animals were also presented as a population mean to show the relative decrease in average calcium response after multiple stimulation periods.

DiSPIM imaging with optical and chemical stimulation. Stimulus control for optical illumination or chemical pulses was integrated with diSPIM volumetric imaging using a custom Micromanager script controlling an Arduino Uno and enabling independent digital switching of 6 TTL channels at the beginning of specified image acquisition timepoints. One TTL channel controlled the intensity of a red LED (617 nm, 3 W, Mightex) connected to the bottom port of the diSPIM and illuminated the sample through a Nikon 4×, 0.1 NA lower objective. A second TTL channel controlled a 12 V fluidic valve system for chemical stimulation (ValveLink 8.2, Automate). Pinch valves allowed flow of either buffer or chemical stimulus lines into the microfluidic channel network, flowing to a common outlet.

For optogenetic stimulation experiments, animals were embedded in BIO-133 disks bonded to a cover glass placed in the diSPIM sample chamber. To embed animals, they were first transiently immobilized by being picked onto seeded (OP50 *E. coli*) plates with 1 mM tetramisole, and allowed to rest for 1.5 hours. Subsequently, worms were picked into a droplet of BIO-133 polymer liquid and gelled in the same manner as the PEG-DA hydrogel disks above, using a TMSPMA silanized coverslip for covalent bonding.

For chemical stimulation experiments, animals were embedded in PEG hydrogel disks. Animals can be maintained in these disks for many hours if they are kept hydrated.[7] Just prior to an experiment, an animal-embedded disk was inserted into the sample cavity of the diSPIM microfluidic chamber. A 75–80 μm thick BIO-133 membrane was sealed to the microfluidic device surface, closing the fluidic channel with the PEG disk and animals contained within. The hydrogel disk was inserted into a droplet of S. basal buffer present in the well to avoid the introduction of bubbles that would disrupt microfluidic flow. To assure continuous microfluidic flow through the chamber without leaking, we balanced inlet and outlet flows by adjusting the reservoir heights. Specifically, inlet reservoir heights were held slightly above the stage (Δh_{in}), and the outlet reservoir level was placed further below the stage ($\Delta h_{out} > \Delta h_{in}$) to ensure a slight negative pressure in the chamber. Microfluidic stimulus switching was achieved using a dual pinch valve (NResearch Inc., 161P091), that alternately allows either a buffer or stimulus line to flow through the microfluidic chamber to the single outflow line.

A typical diSPIM acquisition captured one volume per second (10 ms exposure, minimum slice time setting, 55 slices per volume, 166.4 × 166.4 × 82.5 μm total volume space) for 10 minutes, with 20 s duration stimulation every minute. Z-Projection time series videos were produced in ImageJ from cropped versions of the total number of images,

then analyzed for GCaMP neural fluorescence using rectangular boxes for integrated fluorescence density, with a nearby region void of signal used for background subtraction.

Author contributions

Conceived project: R. P., H. S. Designed experiments: X. H., Y. S., H. W., K. M. O., H. D. V., E. G., D. A., R. P., H. S. Provided technical advice and resources for microfluidics: N. M., R. P., H. W., D. A. Provided biological advice: R. C., Y. S., S. H., Y. P. Created new reagents: S. H., Y. P., M. W. M. Performed experiments: X. H., Y. S., H. W., K. M. O., D. P., H. D. V., R. P. Tracked nuclei in GCaMP imaging experiments: X. H., Y. S., S. X. Wrote paper with input from all authors: X. H., Y. S., H. W., D. A., R. P., H. S. Supervised research: Q. D., Y. P., E. G., D. A., R. P., H. S. Directed research: H. S.

Data availability

The data that support the findings of this study are available from the corresponding author upon reasonable request.

Conflicts of interest

The authors declare no conflict of interest. The NIH, its officers, and staff do not recommend or endorse any company, product, or service.

Acknowledgements

This research was funded in part by the National Institute of Biomedical Imaging and Bioengineering, the National Institute of Neurological Disorders and Stroke, and the Center for Cancer Research of the National Cancer Institute within the National Institutes of Health (Z01 BC 006161), and the National Science Foundation (CBET 1605679). We thank George Patterson for the use of his cell culture facilities, Leighton Duncan and Daniel Colón-Ramos for kindly providing strains and for conducting initial pilot experiments and their careful read, Evan Ardiel and Eviatar Yemini for providing helpful feedback on pan-nuclear GCaMP recordings, Ron Zohar and Ehud Shchori for providing useful information on BIO-133, and Hank Eden for providing helpful feedback on the manuscript. K.M.O. and E.G. were supported by NINDS Z01-NS003013 to E. G. and K. M. O. was also jointly supported by AFOSR grant number FA9550-16-1-0052 to W. Losert at UMD College Park. M. W. M was supported by NIH grant F32-NS098616.

References

1 M. Chalfie, Y. Tu, G. Euskirchen, W. W. Ward and D. C. Prasher, Green fluorescent protein as a marker for gene expression, *Science*, 1994, **263**, 802–805.
2 G. Ou, N. Stuurman, M. D'Ambrosio and R. D. Vale, Polarized Myosin Produces Unequal-Size Daughters During Asymmetric Cell Division, *Science*, 2010, **330**, 677–680.
3 S. Kato, *et al.*, Global brain dynamics embed the motor command sequence of Caenorhabditis elegans, *Cell*, 2015, **163**, 656–669.
4 T. V. Chokshi, A. Ben-Yakar and N. Chronis, CO2 and compressive immobilization of C. elegans on-chip, *Lab Chip*, 2009, **9**, 151–157.
5 J. J. Snow, *et al.*, Two anterograde intraflagellar transport motors cooperate to build sensory cilia on C. elegans neurons, *Nat. Cell Biol.*, 2004, **6**, 1109–1113.
6 E. Kim, L. Sun, C. V. Gabel and C. Fang-Yen, Long-Term Imaging of Caenorhabditis elegans Using Nanoparticle-Mediated Immobilization, *PLoS One*, 2013, e53419.
7 K. Burnett, E. Edsinger and D. R. Albrecht, Rapid and gentle hydrogel encapsulation of living organisms enables long-term microscopy over multiple hours, *Commun. Biol.*, 2018, **1**, 73.
8 C. B. Rohde, F. Zeng, R. Gonzalez-Rubio, M. Angel and M. F. Yanik, Microfluidic system for on-chip high-throughput whole-animal sorting and screening at subcellular resolution, *Proc. Natl. Acad. Sci. U. S. A.*, 2007, **104**, 13891–13895.
9 M. Cornaglia, T. Lehnert and M. A. M. Gijs, Microfluidic systems for high-throughput and high-content screening using the nematode Caenorhabditis elegans, *Lab Chip*, 2017, **17**, 3736–3759.
10 S. Berger, *et al.*, Long-term C. elegans immobilization enables high resolution developmental studies in vivo, *Lab Chip*, 2018, **18**, 1359–1368.
11 S. Mondal, *et al.*, Large-scale microfluidics providing high-resolution and high-throughput screening of Caenorhabditis elegans poly-glutamine aggregation model, *Nat. Commun.*, 2016, **7**, 13023.
12 T. J. Levario, M. Zhan, B. Lim, S. Y. Shvartsman and H. Lu, Microfluidic trap array for massively parallel imaging of Drosophila embryos, *Nat. Protoc.*, 2013, **8**, 721–736.
13 M. F. Yanik, C. B. Rohde and C. Pardo-Martin, Technologies for micromanipulating, imaging, and phenotyping small invertebrates and vertebrates, *Annu. Rev. Biomed. Eng.*, 2011, **13**, 185–217.
14 A. Z. Shorr, U. M. Sönmez, J. S. Minden and P. R. LeDuc, High-throughput mechanotransduction in Drosophila embryos with mesofluidics, *Lab Chip*, 2019, **19**, 1141–1152.
15 S. Stavrakis, G. Holzner, J. Choo and A. DeMello, High-throughput microfluidic imaging flow cytometry, *Curr. Opin. Biotechnol.*, 2018, **55**, 36–43.
16 R. Probst, Z. Cummins, C. Ropp, E. Waks and B. Shapiro, Flow Control of Small Objects On-Chip: Manipulating Live Cells, Quantum Dots, and Nano-Wires, *IEEE Control Systems Magazine*, 2012, **32**, 26–53.
17 J. Riba, J. Schoendube, S. Zimmermann, P. Koltay and R. Zengerle, Single-cell dispensing and 'real-time' cell classification using convolutional neural networks for higher efficiency in single-cell cloning, *Sci. Rep.*, 2020, **10**, 1193.

18 V. Anagnostidis, *et al.*, Deep learning guided image-based droplet sorting for on-demand selection and analysis of single cells and 3D cell cultures, *Lab Chip*, 2020, **20**, 889–900.
19 J. Lam, *et al.*, Adaptation of a Simple Microfluidic Platform for High-Dimensional Quantitative Morphological Analysis of Human Mesenchymal Stromal Cells on Polystyrene-Based Substrates, *SLAS Technol.*, 2017, **22**, 646–661.
20 M. T. Doolin and K. M. Stroka, Integration of Mesenchymal Stem Cells into a Novel Micropillar Confinement Assay, *Tissue Eng., Part C*, 2019, **25**, 662–676.
21 D. R. Albrecht, *et al.*, Microfluidics-integrated time-lapse imaging for analysis of cellular dynamics, *Integr. Biol.*, 2010, **2**, 278–287.
22 D. K. Reilly, D. E. Lawler, D. R. Albrecht and J. Srinivasan, Using an Adapted Microfluidic Olfactory Chip for the Imaging of Neuronal Activity in Response to Pheromones in Male C. Elegans Head Neurons, *J. Visualized Exp.*, 2017, **127**, e56026.
23 E. Yemini, *et al.*, NeuroPAL: A Neuronal Polychromatic Atlas of Landmarks for Whole-Brain Imaging in C. elegans, *bioRxiv*, 2019, DOI: 10.1101/676312.
24 I. D.-C. Cáceres, N. Valmas, M. A. Hilliard and H. Lu, Laterally Orienting C. elegans Using Geometry at Microscale for High-Throughput Visual Screens in Neurodegeneration and Neuronal Development Studies, *PLoS One*, 2012, **7**, e35037.
25 D. R. Albrecht and C. I. Bargmann, High-content behavioral analysis of Caenorhabditis elegans in precise spatiotemporal chemical environments, *Nat. Methods*, 2011, **8**, 599–605.
26 S. J. Belfer, *et al.*, Caenorhabditis-in-Drop Array for Monitoring C. elegans Quiescent Behavior, *Sleep*, 2013, **36**, 689–698.
27 M. Scholz, D. J. Lynch, K. S. Lee, E. Levine and D. Biron, A scalable method for automatically measuring pharyngeal pumping in C. elegans, *J. Neurosci. Methods*, 2016, **274**, 172–178.
28 H. B. Atakan, M. Cornaglia, L. Mouchiroud, J. Auwerx and M. A. M. Gijs, Automated high-content phenotyping from the first larval stage till the onset of adulthood of the nematode Caenorhabditis elegans, *Lab Chip*, 2018, **19**, 120–135.
29 S. E. Hulme, *et al.*, Lifespan-on-a-chip: microfluidic chambers for performing lifelong observations of C. elegans, *Lab Chip*, 2010, **10**, 589–597.
30 H. Hwang, J. Krajniak, Y. Matsunaga, G. M. Benian and H. Lu, On-demand optical immobilization of Caenorhabditis elegans for high-resolution imaging and microinjection, *Lab Chip*, 2014, **14**, 3498–3501.
31 J. Krajniak and H. Lu, Long-term high-resolution imaging and culture of C. elegans in chip-gel hybrid microfluidic device for developmental studies, *Lab Chip*, 2010, **10**, 1862–1868.
32 S. Nam, R. Stowers, J. Lou, Y. Xia and O. Chaudhuri, Varying PEG density to control stress relaxation in alginate-PEG hydrogels for 3D cell culture studies, *Biomaterials*, 2019, **200**, 15–24.
33 Z. F. Zhang, X. Ma, H. Wang and F. Ye, Influence of polymerization conditions on the refractive index of poly(ethylene glycol) diacrylate (PEGDA) hydrogels, *Appl. Phys. A: Mater. Sci. Process.*, 2018, **124**, 283.
34 N. R. Wevers, *et al.*, High-throughput compound evaluation on 3D networks of neurons and glia in a microfluidic platform, *Sci. Rep.*, 2016, **6**, 38856.
35 W. E. Pittman, D. B. Sinha, W. B. Zhang, H. E. Kinser and Z. Pincus, A simple culture system for long-term imaging of individual C. elegans, *Lab Chip*, 2017, **17**, 3909–3920.
36 D. N. H. Kim, K. T. Kim, C. Kim, M. A. Teitell and T. A. Zangle, Soft lithography fabrication of index-matched microfluidic devices for reducing artifacts in fluorescence and quantitative phase imaging, *Microfluid. Nanofluid.*, 2017, **22**, 2.
37 E. R. Polanco, N. Western and T. A. Zangle, Fabrication of Refractive-index-matched Devices for Biomedical Microfluidics, *J. Visualized Exp.*, 2018, **139**, 58296.
38 T. J. Levario, P. Insley, H. Hwang, S. Shaham and H. Lu, in *18th International Conference on Miniaturized Systems for Chemistry and Life Sciences, MicroTAS 2014*, San Antonio, TX, 2014, pp. 727–729.
39 T. Xu, *et al.*, Modified inverted selective plane illumination microscopy for sub-micrometer imaging resolution in polydimethylsiloxane soft lithography devices, *Lab Chip*, 2020, **20**, 3960–3969, DOI: 10.1039/d0lc00598c.
40 T.-Y. Chang, C. Pardo-Martin, A. Allalou, C. Wählby and M. F. Yanik, Fully automated cellular-resolution vertebrate screening platform with parallel animal processing, *Lab Chip*, 2012, **12**, 711–716.
41 M. Tonin, N. Descharmes and R. Houdré, Hybrid PDMS/glass microfluidics for high resolution imaging and application to sub-wavelength particle trapping, *Lab Chip*, 2016, **16**, 465–470.
42 D. Turaga and T. E. Holy, Miniaturization adn defocus correction for objective-coupled planar illumination microscopy, *Opt. Lett.*, 2008, **33**, 2302–2304.
43 Y. Wu, *et al.*, Spatially isotropic four-dimensional imaging with dual-view plane illumination microscopy, *Nat. Biotechnol.*, 2013, **31**, 1032–1038.
44 B. C. Chen, *et al.*, Lattice light-sheet microscopy: imaging molecules to embryos at high spatiotemporal resolution, *Science*, 2014, **346**, 1257998.
45 P. N. Hedde, L. Malacrida, S. Ahrar, A. Siryaporn and E. Gratton, sideSPIM - selective plane illumination based on a conventional inverted microscope, *Biomed. Opt. Express*, 2017, **8**, 3918–3937.
46 A. Kumar, *et al.*, Dual-view plane illumination microscopy for rapid and spatially isotropic imaging, *Nat. Protoc.*, 2014, **9**, 2555–2573.
47 A. Kaufmann, M. Mickoleit, M. Weber and J. Huisken, Multilayer mounting enables long-term imaging of zebrafish development in a light sheet microscope, *Development*, 2012, **139**, 3242–3247.

48 A. G. York, *et al.*, Instant super-resolution imaging in live cells and embryos via analog image processing, *Nat. Methods*, 2013, **10**, 1122–1126.
49 M. A. Murray, M. Schubiger and J. Palka, Neuron Differentiation and Axon Growth in the Developing Wing of Drosophila melanogaster, *Dev. Biol.*, 1984, **104**, 259–273.
50 Y. N. Jan, A. Ghysen, I. Christoph, S. Barbel and L. Y. Jan, Formation of Neuronal Pathways in the Imaginal Discs of Drosophila melanogaster, *J. Neurosci.*, 1985, **5**, 2453–2464.
51 A. Clarke, *et al.*, Dynamic Morphogenesis of a Pioneer Axon in Drosophila and Its Regulation by Abl Tyrosine Kinase, *Mol. Biol. Cell*, 2020, **31**, 452–465.
52 A. Clarke, *et al.*, Abl Signaling Directs Growth of a Pioneer Axon in Drosophila by Shaping the Intrinsic Fluctuations of Actin, *Mol. Biol. Cell*, 2020, **31**, 466–477.
53 S. E. Hulme, S. S. Shevkoplyas, J. Apfeld, W. Fontana and G. Whitesides, A Microfabricated Array of Clamps for Immobilizing and Imaging C. Elegans, *Lab Chip*, 2007, **7**, 1515–1523.
54 M. Guo, *et al.*, Rapid image deconvolution and multiview fusion for optical microscopy, *Nat. Biotechnol.*, 2020, **38**, 1337–1346, DOI: 10.1038/s41587-020-0560-x.
55 T.-W. Chen, *et al.*, Ultra-sensitive fluorescent proteins for imaging neuronal activity, *Nature*, 2013, **499**, 295–300.
56 J. P. Nguyen, A. N. Linder, G. S. Plummer, J. W. Shaevitz and A. M. Leifer, Automatically tracking neurons in a moving and deforming brain, *PLoS Comput. Biol.*, 2017, **13**, e1005517.
57 J. Larsch, D. Ventimiglia, C. I. Bargmann and D. R. Albrecht, High-throughput imaging of neuronal activity in Caenorhabditis elegans, *Proc. Natl. Acad. Sci. U. S. A.*, 2013, **110**, E4266–4273.
58 P. Sengupta, J. H. Chou and C. I. Bargmann, odr-10 Encodes a Seven Transmembrane Domain Olfactory Receptor Required for Responses to the Odorant Diacetyl, *Cell*, 1996, **84**, 899–909.
59 H. Shidara, K. Hotta and K. Oka, Compartmentalized cGMP Responses of Olfactory Sensory Neurons in Caenorhabditis elegans, *J. Neurosci.*, 2017, **37**, 3753–3763.
60 N. C. Klapoetke, *et al.*, Independent optical excitation of distinct neural populations, *Nat. Methods*, 2014, **11**, 338–346.
61 C. Martin, *et al.*, Line excitation array detection fluorescence microscopy at 0.8 million frames per second, *Nat. Commun.*, 2018, **9**, 4499.
62 Y. Han, *et al.*, Cameraless high-throughput three-dimensional imaging flow cytometry, *Optica*, 2019, **6**, 1297–1304.
63 A. Ravasio, S. Vaishnavi, B. Ladoux and V. Viasnoff, High-resolution imaging of cellular processes across textured surfaces using an index-matched elastomer, *Acta Biomater.*, 2015, **14**, 53–60.
64 F. Xiao, X. Wen, X. H. M. Tan and P.-Y. Chiou, Plasmonic micropillars for precision cell force measurements across a large field-of-view, *Appl. Phys. Lett.*, 2018, **112**, 033701.
65 D. C. Duffy, J. C. McDonald, O. J. Schueller and G. M. Whitesides, Rapid Prototyping of Microfluidic Systems in Poly(dimethylsiloxane), *Anal. Chem.*, 1998, **70**, 4974–4984.
66 M. Guo, *et al.*, Single-shot super-resolution total internal reflection fluorescence microscopy, *Nat. Methods*, 2018, **15**, 425–428.
67 A. Descloux, K. S. Grußmayer and A. Radenovic, Parameter-free image resolution estimation based on decorrelation analysis, *Nat. Methods*, 2019, **16**, 918–924.
68 Y. Xia and G. M. Whitesides, Soft Lithography, *Angew. Chem., Int. Ed.*, 1998, **37**, 550–575.
69 J. Atencia, *et al.*, Magnetic connectors for microfluidic applications, *Lab Chip*, 2010, **10**, 246–249.
70 A. D. Edelstein, *et al.*, Advanced methods of microscope control using μManager software, *J. Biol. Methods*, 2014, **1**, e11.
71 E. L. Ardiel, *et al.*, Visualizing Calcium Flux in Freely Moving Nematode Embryos, *Biophys. J.*, 2017, **112**, 1975–1983.
72 R. C. Lagoy and D. R. Albrecht, Microfluidic Devices for Behavioral Analysis, Microscopy, and Neuronal Imaging in Caenorhabditis elegans, *Methods Mol. Biol.*, 2015, **1327**, 159–179.
73 R. C. Lagoy and D. R. Albrecht, Automated fluid delivery from multiwell plates to microfluidic devices for high-throughput experiments and microscopy, *Sci. Rep.*, 2018, **8**, 6217.

Electronic Supplementary Material (ESI) for Lab on a Chip.

Supplementary Video 1, Mitochondrial dynamics imaged at isotropic resolution with diSPIM, through 50 μm of BIO-133. U2OS cells expressing mEmerald-Tomm20 were imaged with diSPIM, acquiring 50 volumes with 3 s inter-volume spacing. Lateral and axial maximum intensity projections of dual-view reconstructions are shown. Higher magnification views of red and yellow rectangular regions at left are shown at right. See also **Fig. 2c, d**.

Supplementary Video 2, Flowing fixed DAPI-labeled U2OS cells, as imaged through 50 μm BIO-133 in diSPIM. Single-view, raw data are shown. See also **Supplementary Fig. 6.**

Supplementary Video 3, Mitochondrial dynamics imaged at super-resolution with iSIM, through 50 μm of BIO-133. U2OS cells expressing mEmerald-Tomm20 were imaged with iSIM, acquiring 25 volumes with 3 s inter-volume spacing. Lateral maximum intensity projections of deconvolved data are shown. A higher magnification view of yellow rectangular regions is also shown. Data have been median filtered for display. See also **Fig. 2f, g.**

Supplementary Video 4, Lysosomal dynamics imaged at super-resolution with iSIM, through 50 μm of BIO-133. HCT-116 cells expressing EGFP-LAMP1 were imaged with iSIM, acquiring 60 volumes with 7 s inter-volume spacing. Lateral maximum intensity projections of deconvolved data are shown. Data have been median filtered for display. See also **Supplementary Fig. 8**.

Supplementary Video 5, Z stack of immunostained Tomm 20, Lamin A/C, and actin obtained with iSIM, through 50 μm of BIO-133. Multiple layers of HCT-116 cells were grown on a BIO-133 film, fixed, immunostained, and imaged with iSIM. Deconvolved images are shown, with three-color merge shown in lower right images. See also **Fig. 2h, i**.

Supplementary Video 6, tdTomato-CD4 in *Drosophila* tissue sandwiched between BIO-133 layers. Single-view diSPIM recordings are shown. 360 volumes were acquired with 5 s inter-volume spacing. The 'red-hot' color map from ImageJ is used for display. See also **Fig. 3b, c.**

Supplementary Video 7, Pan-neuronal GCaMP6s dynamics imaged at isotropic resolution in immobilized *C. elegans* adults with diSPIM. Dual-view deconvolved results (GCaMP channel) at 1.25 volumes/s are shown at left, with segmented, tracked dR/R from 126 nuclei shown at right. Lateral and axial views are shown. See also **Fig. 3e-g**.

Supplementary Video 8, Pan-neuronal GCaMP6s dynamics imaged in immobilized larval *C. elegans*. Single-view diSPIM recordings at 4 volumes/s are shown at left (GCaMP channel), with segmented, tracked dR/R from 110 nuclei shown at right. Lateral maximum intensity projections are shown. See also **Fig. 3h-j.**

Supplementary Video 9, Effect of 0.05 mM CCCP on mitochondrial dynamics, as assayed at isotropic resolution with diSPIM, with BIO-133 microfluidics. U2OS cells expressing mEmerald-Tomm20 were imaged with diSPIM, acquiring 90 volumes with 60 s inter-volume spacing. One BIO-133 well was exposed to 0.05 mM CCCP (left), and another was not (control). Maximum intensity projections of dual-view reconstructions are shown. See also **Fig. 4b, c**.

Supplementary Video 10, Single-cell GCaMP dynamics under 1.1 μM diacetyl stimulation in immobilized *C. elegans.* Single-view diSPIM recordings are shown. Lateral maximum intensity projections are shown. See also **Fig. 4f, g.**

Supplementary Video 11, Single-cell GCaMP dynamics under repetitive optogenetic stimulation in *C. elegans* encapsulated in BIO-133. Single-view diSPIM recordings are shown. Lateral maximum intensity projections are shown. See also **Fig. 4h, i.**

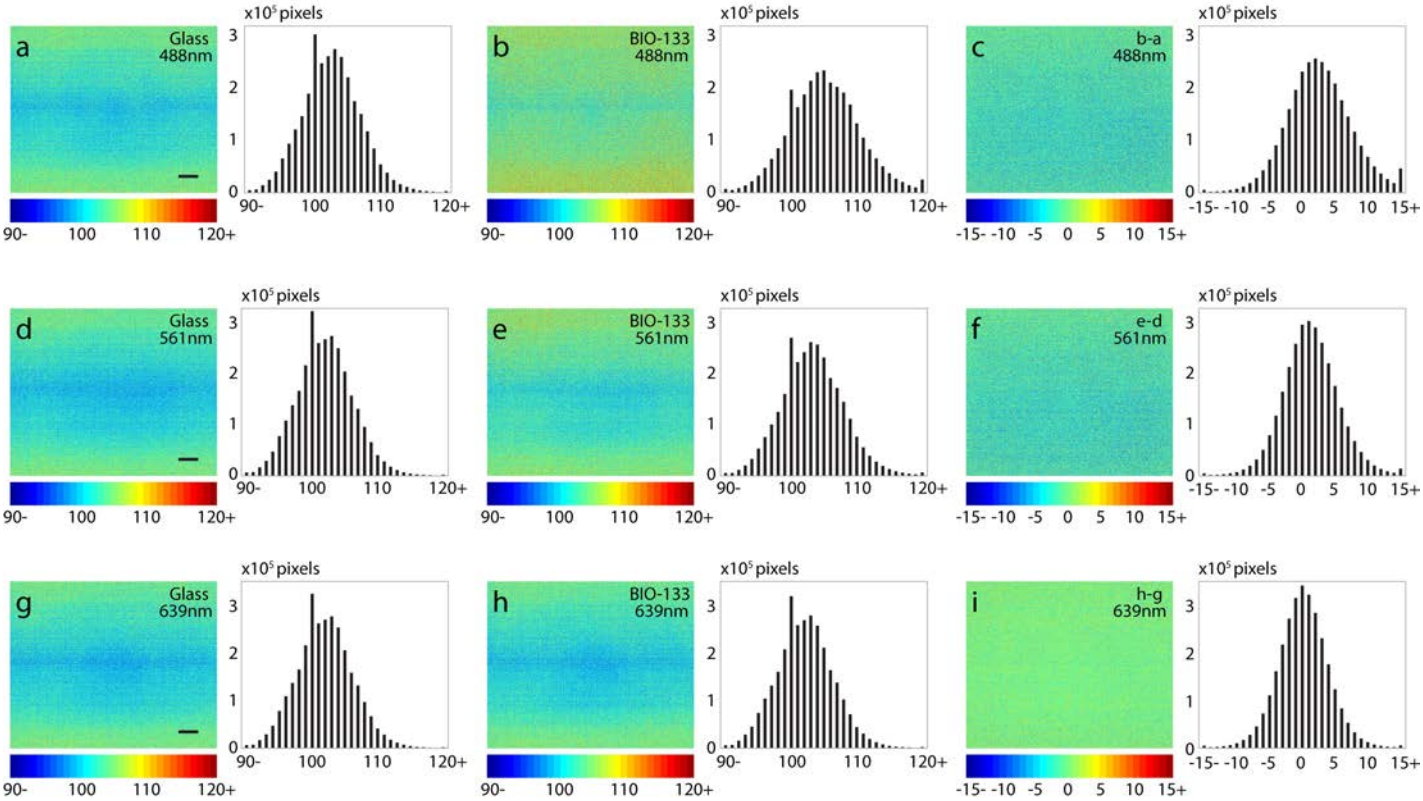

Supplementary Fig. 1, **BIO-133 introduces negligible autofluorescence**. **a)** Image of bare glass coverslip (left) and its associated histogram of counts (right). **b)** As in **a)** but for BIO-133 and its histogram. **c)** Difference image between the two images **b)** - **a)** and associated histogram. Images were acquired with instant SIM using 488 nm excitation and 45 mW excitation. **d-f)** As in **a-c)** but using 70 mW 561 nm excitation. **g-i**) As in **a-c)** but using 90 mW 639 nm excitation. Scale bars: 10 μm.

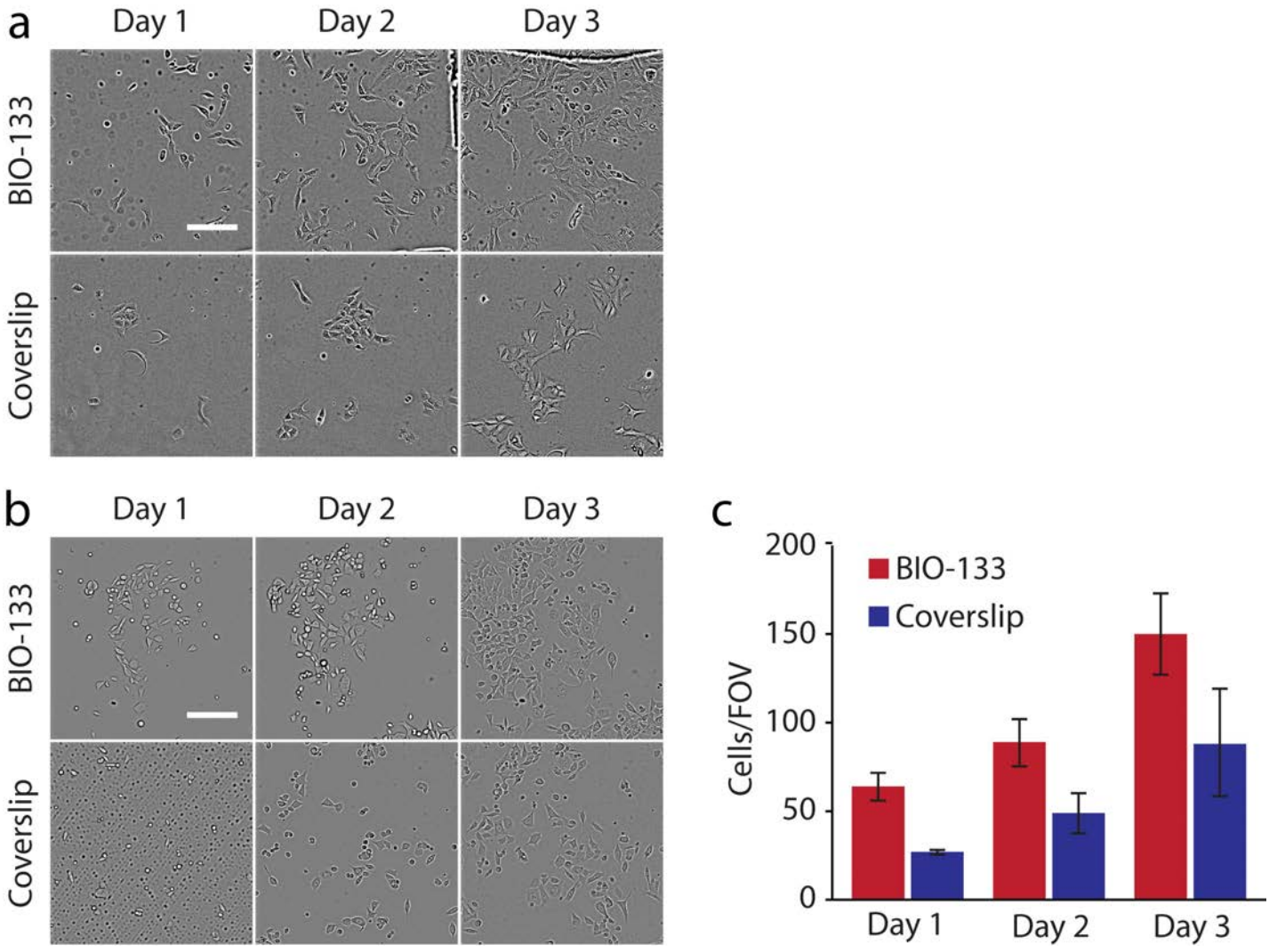

Supplementary Fig. 2, Cells grown on BIO-133 exhibit similar morphology and growth rate to cells grown on glass coverslips. a) U2OS cell growth over 3 days, on BIO-133 (top row) and glass (bottom row). **b)** As in **a)**, but for HCT-116 TOP1-GFP cells. **c)** Quantifying HCT-116 TOP1-GFP cell growth on 50 μm thick BIO-133 layer vs. glass coverslip. Means and standard deviations from 3 fields of view are shown. Brightfield images are shown after flat-fielding. See also **Fig. 2a**. Scale bar: 200 μm.

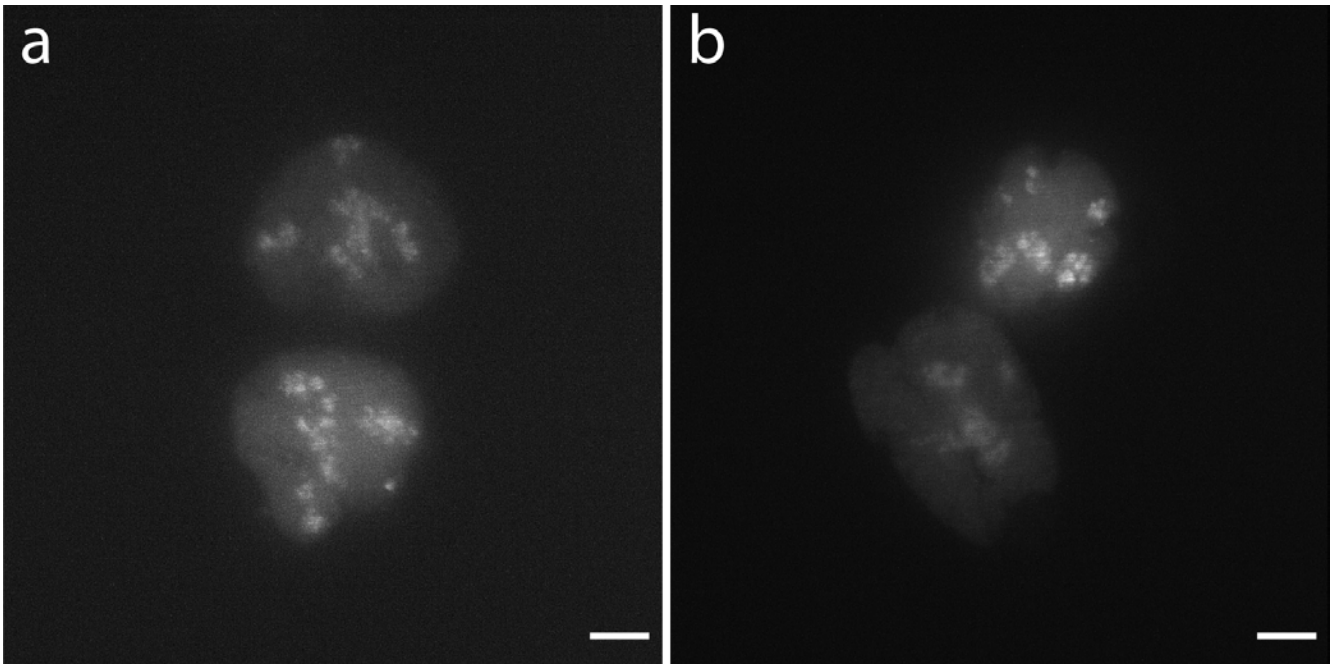

Supplementary Fig. 3, Endogenous expression and localization of topoisomerase I-GFP in HCT-116 TOP1-GFP cells cultured on BIO-133 is comparable to cells grown on glass coverslips. Deconvolved maximum intensity projection of iSIM volume showing endogenous expression and localization of topoisomerase I-GFP in HCT-116 TOP1-GFP cells cultured on glass surface **a)** or BIO-133 surface **b)**. Scale bar: 5 μm.

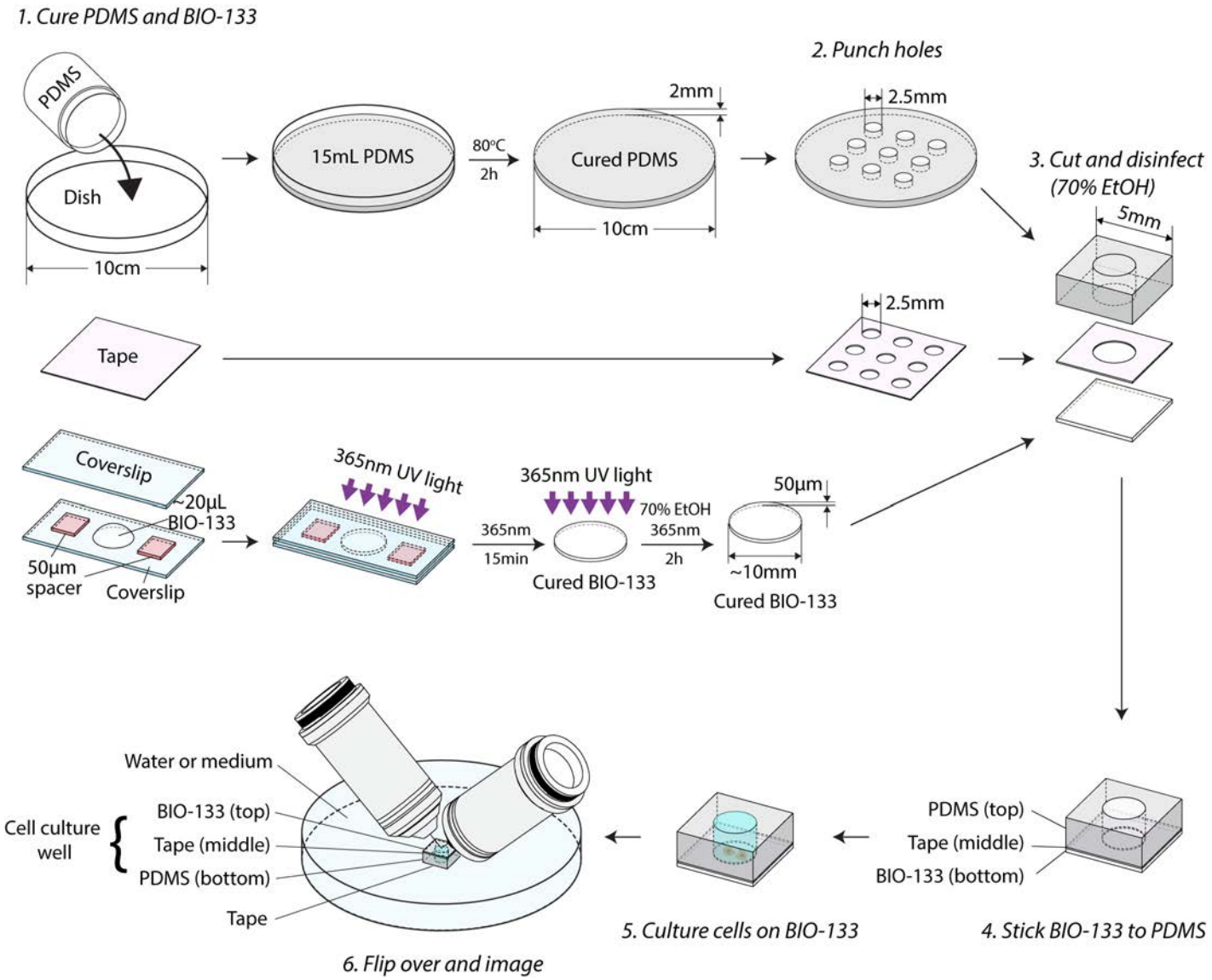

Supplementary Fig. 4, Fabricating BIO-133-sided substrates for cell culture and diSPIM imaging. 1) Cure a PDMS slab and a thin BIO-133 film. 2) Punch wells into PDMS and punch holes on a double-sided tape. 3) Cut PDMS, Tape and BIO-133 into desired shape, disinfect. 4) BIO-133 is adhered to PDMS via adhesive tape. 5) Cells are seeded and cultured on BIO-133 film. 6) The assembly is flipped over and imaged in diSPIM.

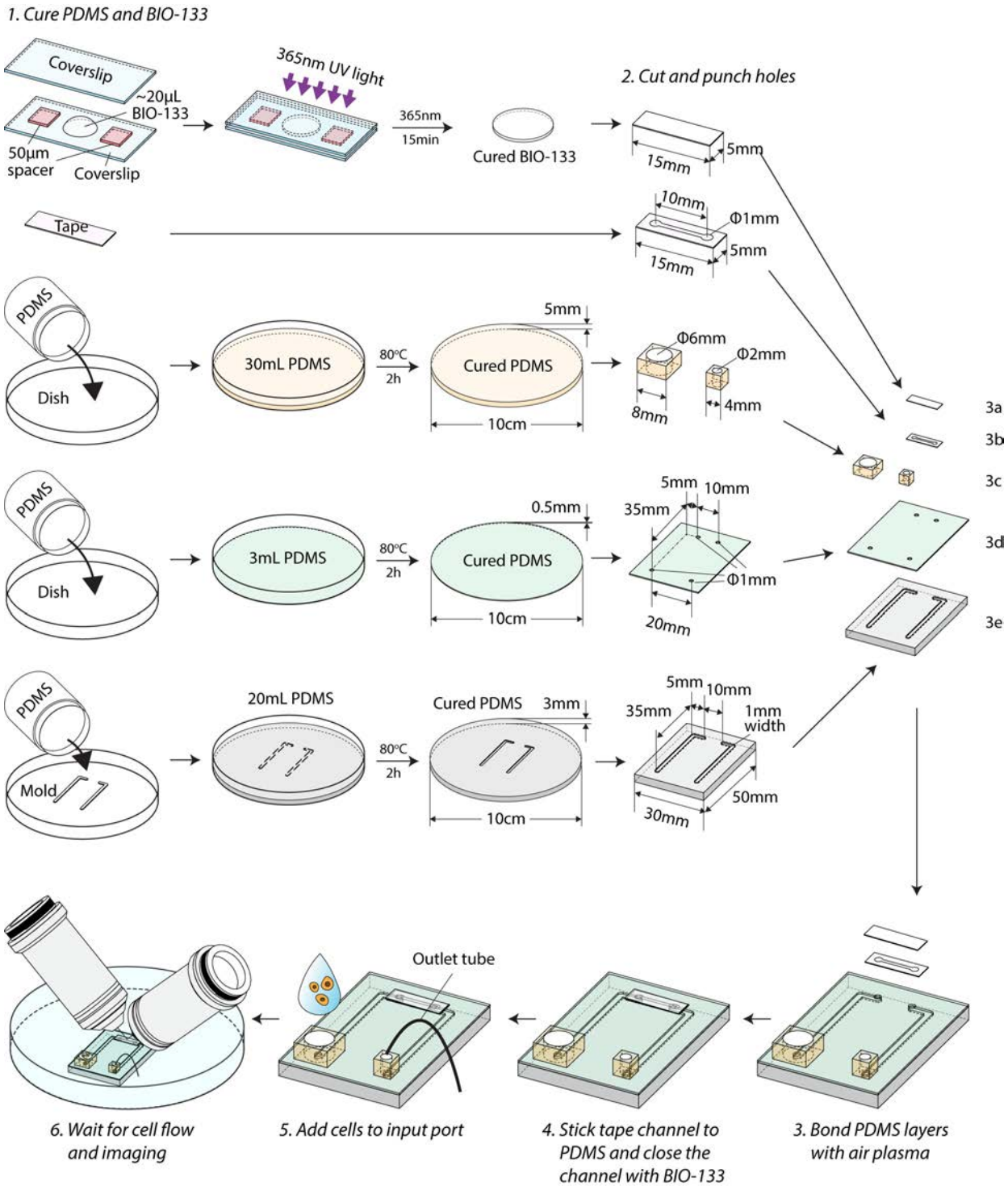

Supplementary Fig. 5, Flow cytometry with BIO-133. 1) Cure BIO-133, a PDMS slab, a thin layer of PDMS and a PDMS with channels. 2) Cut to desired shape and punch holes. Note that holes at the ends of the PDMS channel can also be punched after plasma treatment. 3) Bond the three PDMS layers with air plasma (3c, 3d, 3e). 4) Stick tape channel (3b) to PDMS to connect the two PDMS channels. Stick BIO-133 (3a) to tape to close the channel. 5) Add cells to input port. 6) Wait for the cells to flow into the tape channel and image.

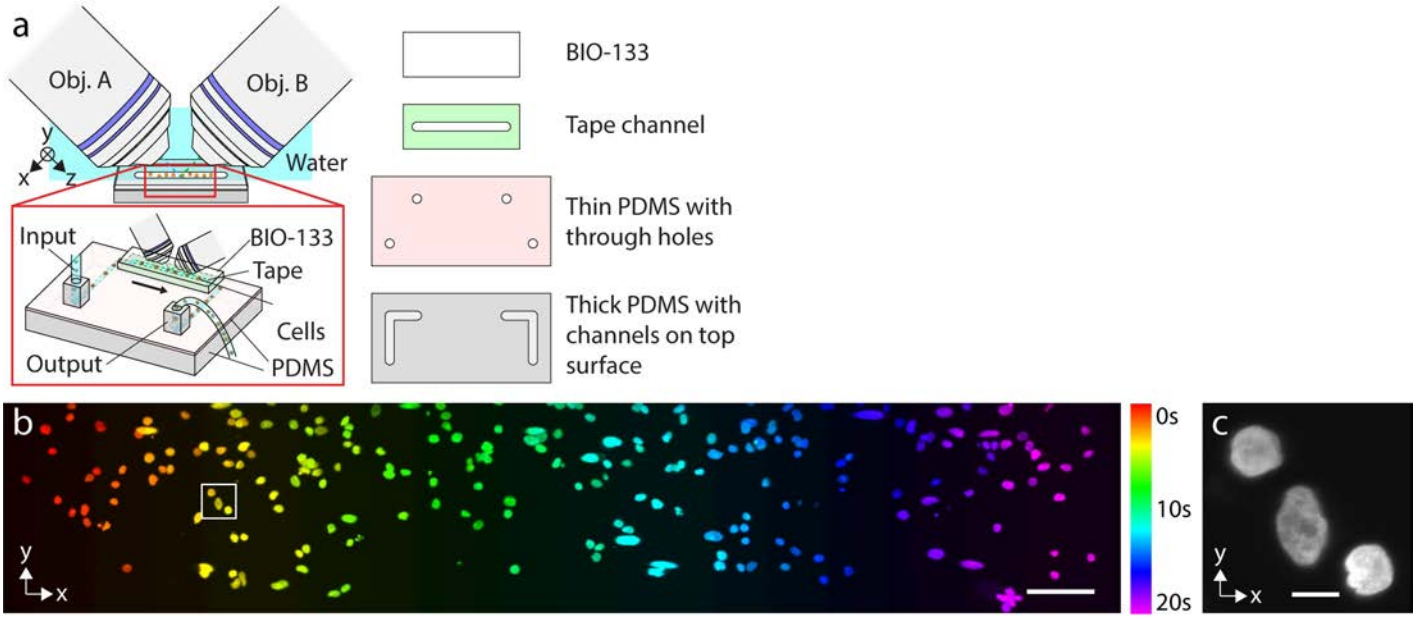

Supplementary Fig. 6, Simple flow cytometry with BIO-133. a) Gravity-driven flow channel with BIO-133 top layer, see also **Methods**. **b)** DAPI-stained nuclei in fixed U2OS cells. Multiple fields of view from 20-s recording are stitched together to show flow vs. time. See also **Supplementary Video 5**. Scale bar: 100 μm. **c)** Higher magnification view of nuclei in white rectangular region in **b)**. Scale bar: 10 μm.

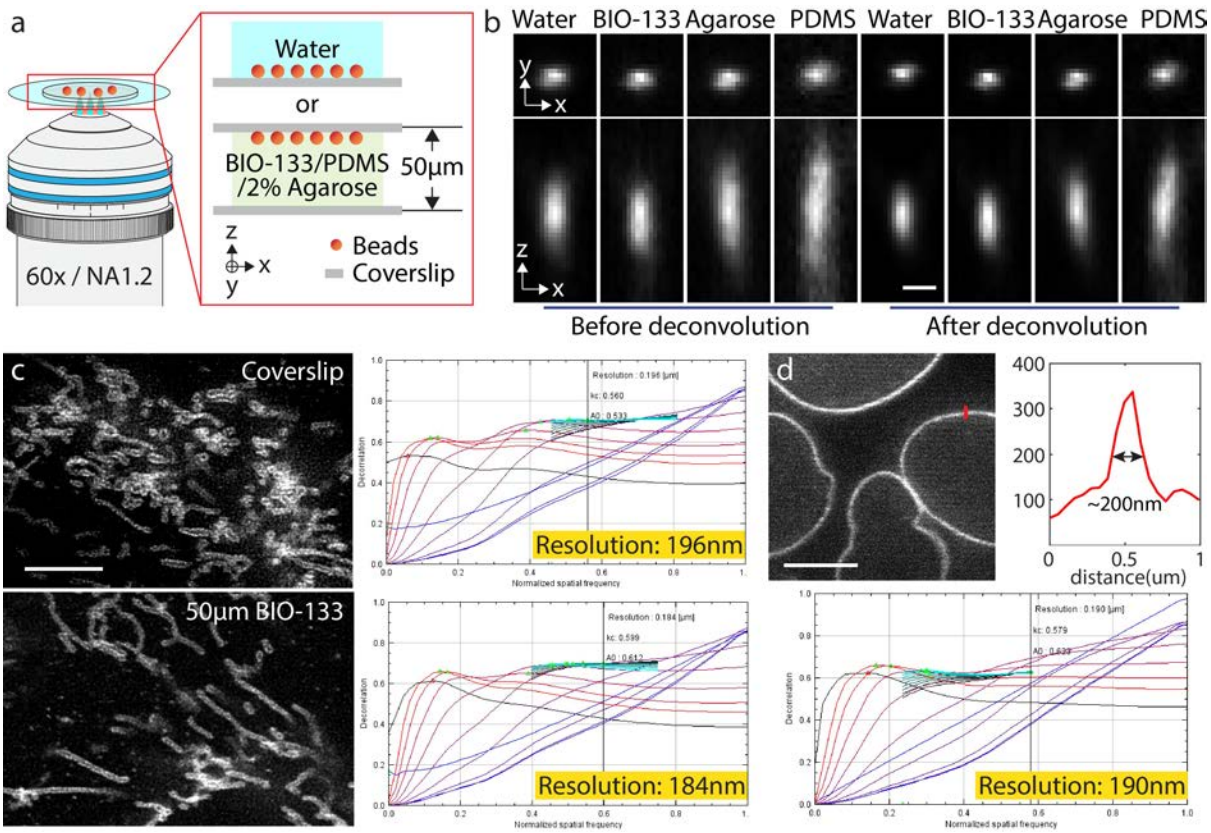

Supplementary Fig. 7, Estimating spatial resolution in iSIM. a) Schematic of PSF estimation, imaging 100 nm beads using iSIM. **b)** xy and xz cross-sections of raw (left four columns) and deconvolved (right four columns) beads. Scale bar: 200 nm. **c)** Decorrelation analysis on Tomm20 images. Top: cells were grown directly on a coverslip. Bottom: cells were grown on and imaged through a 50 µm BIO-133 membrane. Images at left, decorrelation analysis at right. Scale bar: 5 µm. **d)** Measurement of the thickness of nuclear membrane (FHWM), across red line in image at left, and corresponding decorrelation analysis based on entire image below. Scale bar: 5 µm. See also **Fig. 2.**

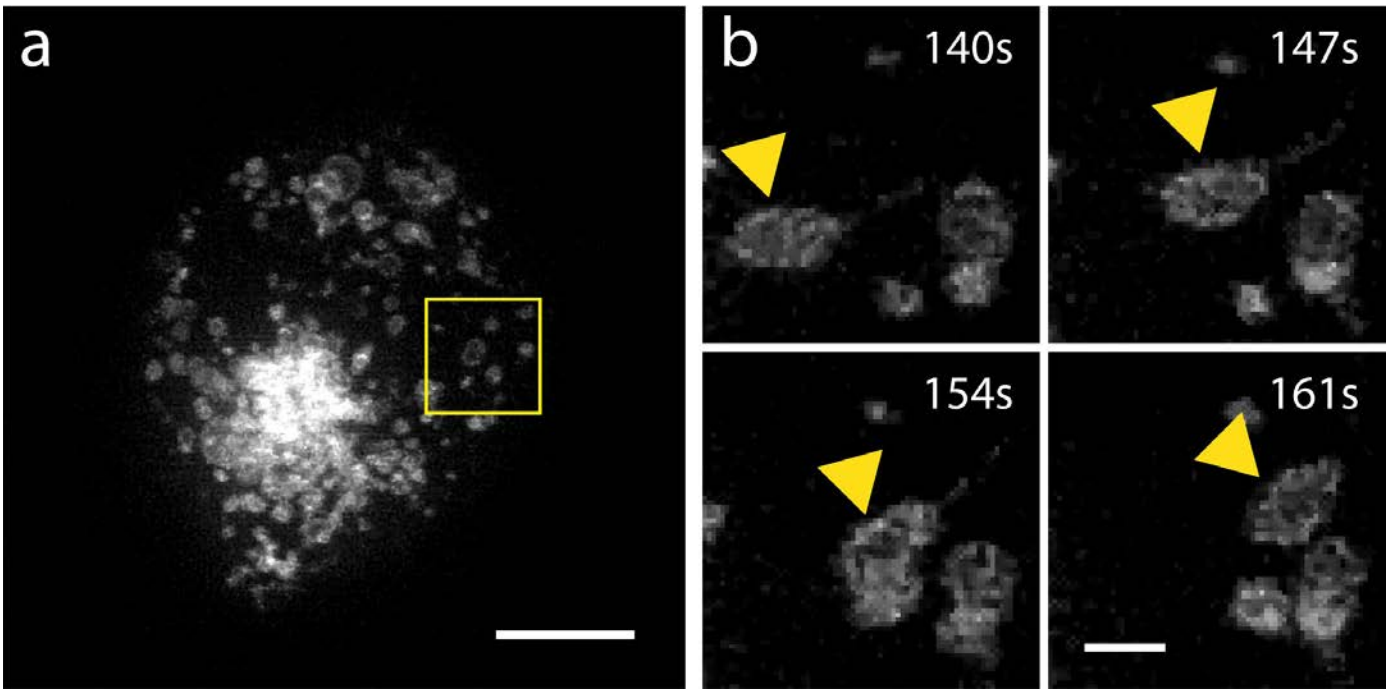

Supplementary Fig. 8, Lysosome dynamics as imaged via iSIM through 50 μm BIO-133. a) Deconvolved maximum intensity projection of iSIM volume showing WT HCT-116 cells expressing EGFP-LAMP1. Scale bar: 5 μm. **b)** Higher magnification view of yellow square rectangular region in **a)**, projected over axial region 9-12 μm from the coverslip. Yellow arrowhead marks the same lysosome. See also **Supplementary Video 4**. Median-filtered data (kernel 0.5 pixel) are shown. Scale bar: 1 μm.

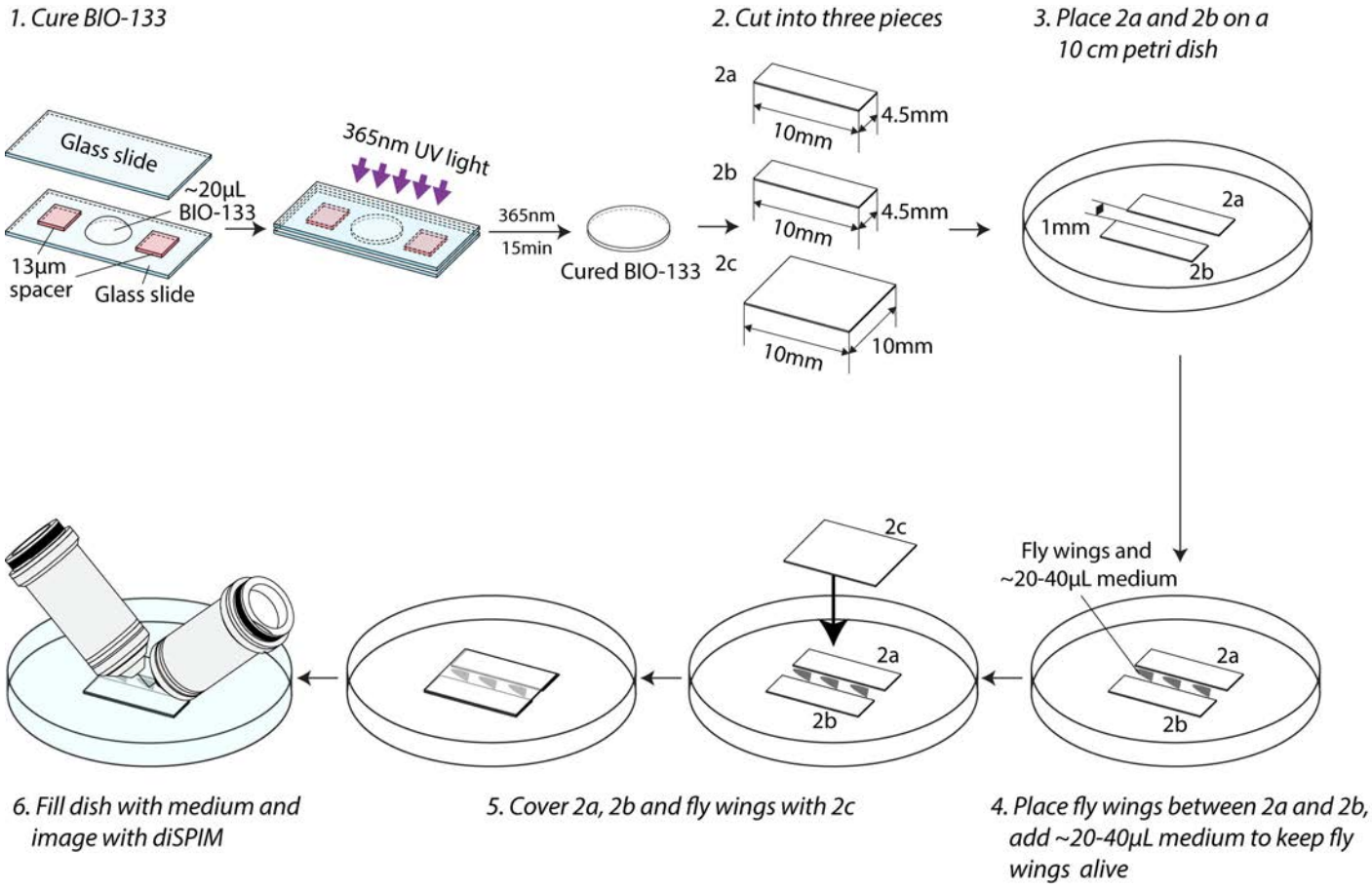

Supplementary Fig. 9, Imaging fly wings in BIO-133 channel with diSPIM. 1) Cure 13 µm thick BIO-133 film. 2) Cut into three pieces (2a, 2b and 2c). 3) Place 2a and 2b directly on a 10 cm petri dish to form a 1 mm wide open-top channel. 4) Place the fly wings between 2a and 2b, add ~20 - 40 µL medium. 5) Cover 2a, 2b and fly wings with 2c. 6) Carefully fill the dish with medium and image with diSPIM.

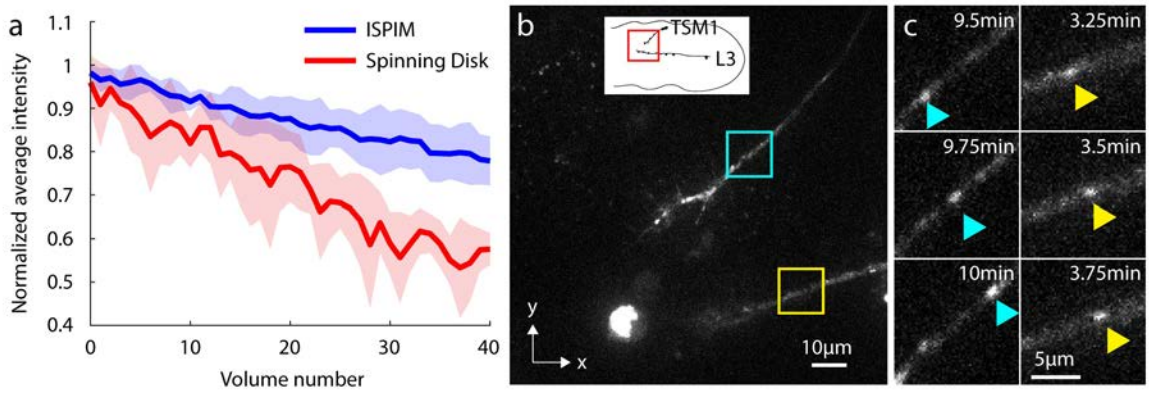

Supplementary Fig. 10, Imaging fly wings with spinning disk confocal microscopy. a) Bleaching comparison between iSPIM (**Fig. 3b**) and spinning disk confocal microscopy. iSPIM volumes were acquired every 5 s with 1 μm axial spacing; spinning disk confocal volumes were acquired every 15 s with 1.3 μm axial spacing. Shaded areas encompass one standard deviation around means (curves); data are pooled from 5 different regions in each dataset. b) Example maximum intensity projection from spinning-disk dataset, indicating TSM1 and L3, labeled with tdTomato-CD4. c) Higher magnification views of blue and yellow rectangles in b), emphasizing trafficking CD4 puncta.

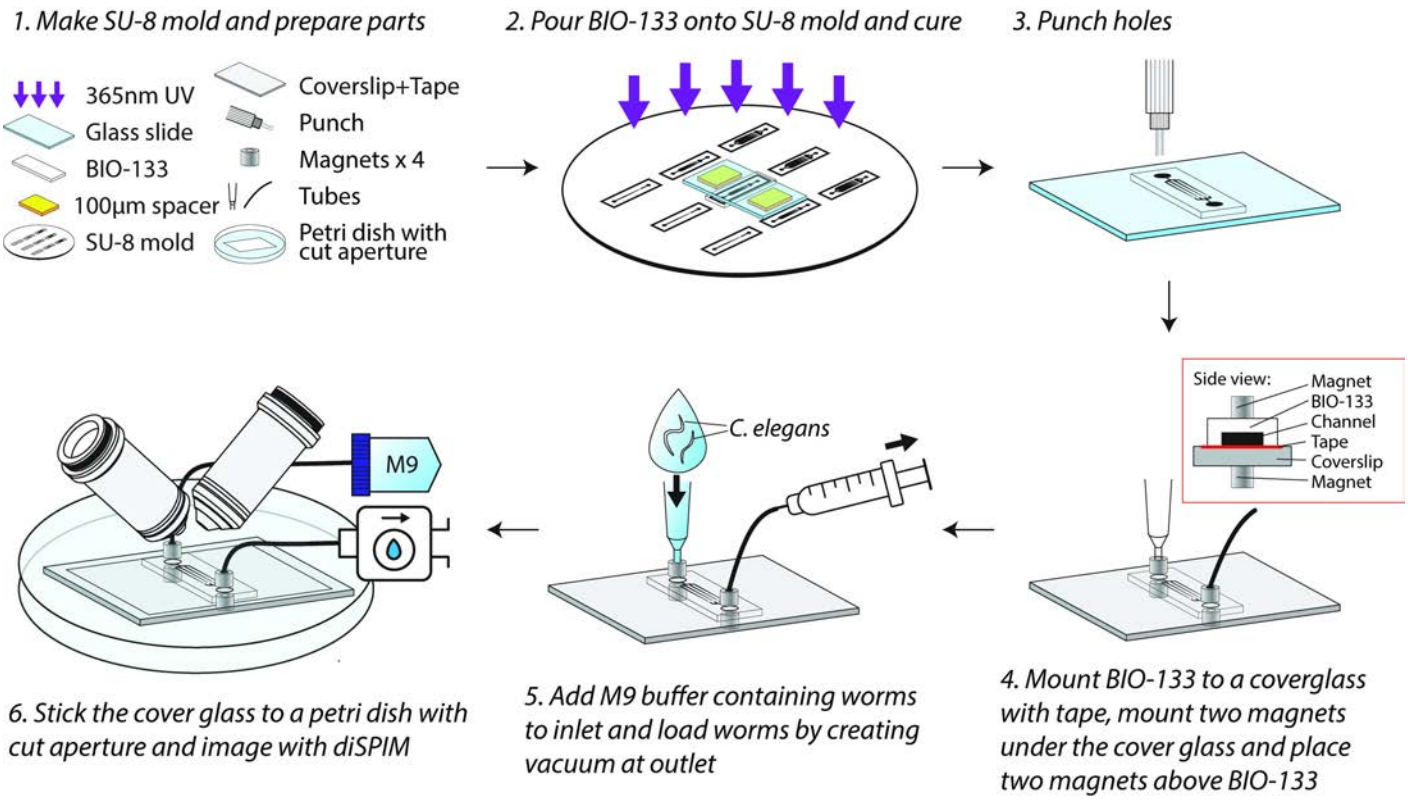

Supplementary Fig. 11, Immobilization and imaging of *C. elegans* in BIO-133 microfluidics. 1) The SU-8 mold and other components are assembled. 2) BIO-133 is poured into the SU-8 mold and cured. 3) The BIO-133 mold is peeled off and holes punched at each end. 4) BIO-133 is mounted to a coverglass with adhesive tape, additionally mounting magnets with tubing for fluid delivery/removal. 5) M9 buffer, worms are added to channels. 6) The assembled microfluidic is placed within a 10 cm petri dish with aperture cut out, covered in water, and imaged with diSPIM.

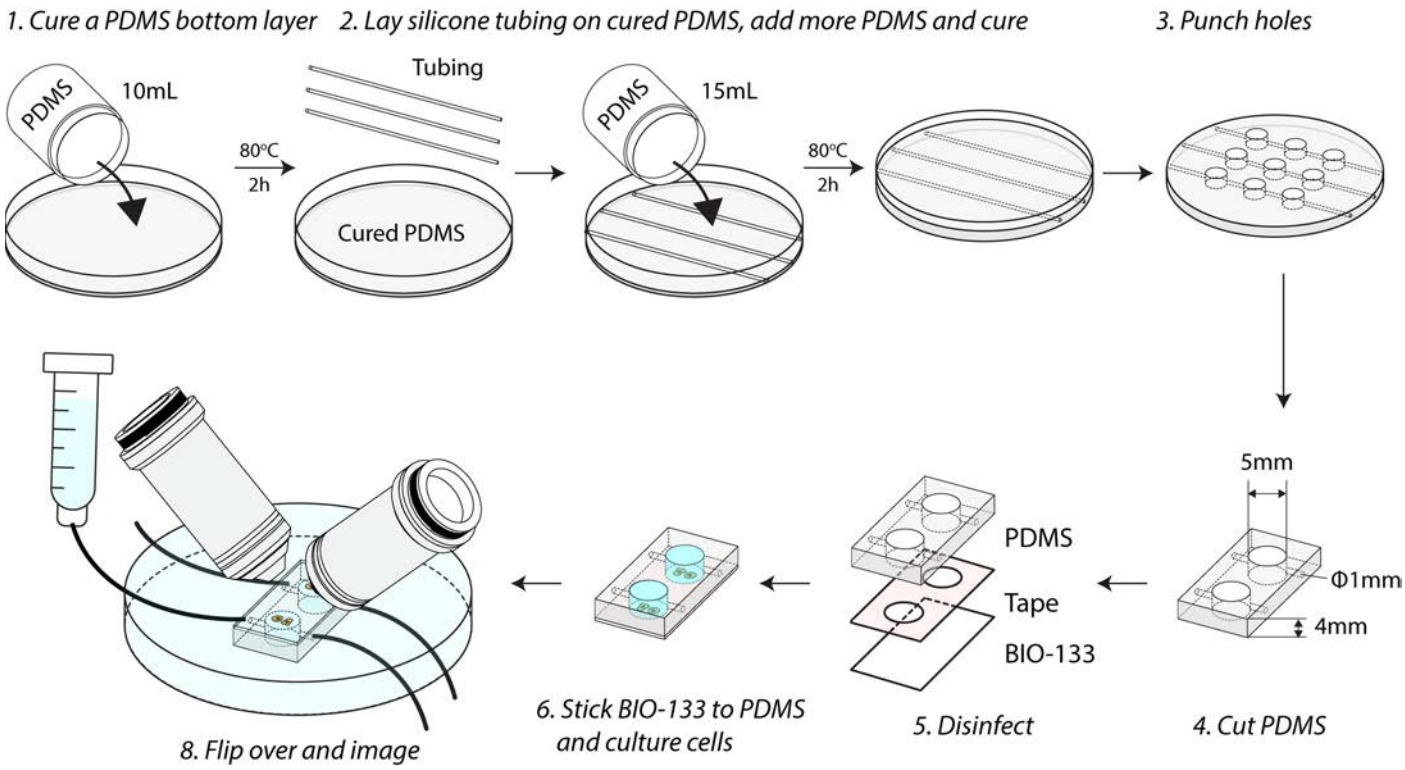

Supplementary Fig. 12, Fabricating BIO-133-sided substrates for chemically stimulating cells. 1) Cure a thin layer of PDMS. 2) Lay silicone tubing on the cured PDMS layer, add more PDMS and cure again to create channels. These channels are used to deliver buffer flow or chemical stimulation and are optional. 3) Wells are punched into PDMS. 4) Cut PDMS into desired shape. 5) Cure BIO-133 film, punch holes on double-sided tape, and put all components in 70% EtOH for disinfection. 6) BIO-133 is adhered to PDMS via adhesive tape; cells are seeded and cultured on BIO-133 film. 7) The assembly is flipped over and imaged in diSPIM. For chemical stimulation, tubing is inserted into PDMS and chemical flow is driven by gravity.

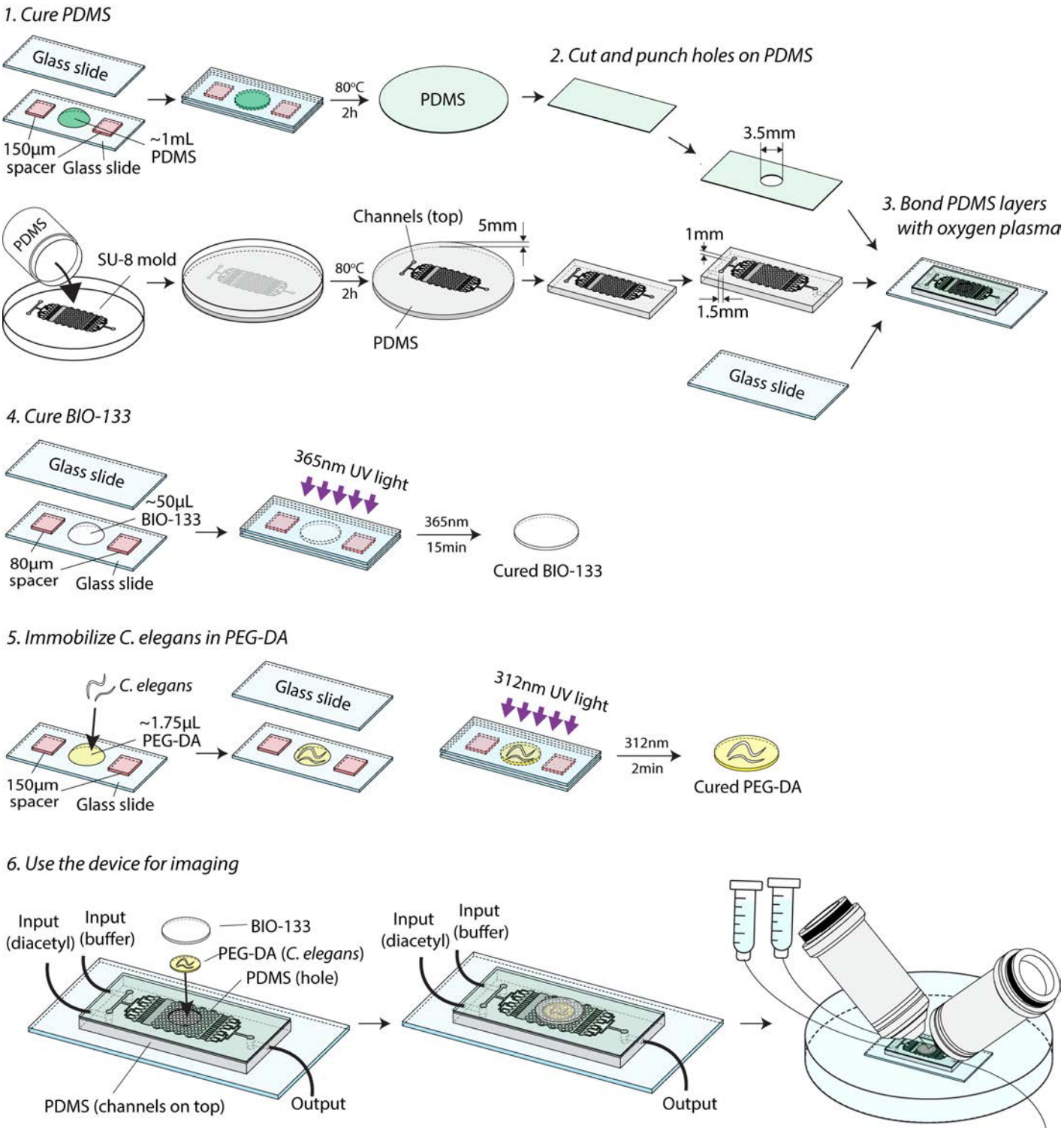

Supplementary Fig. 13, Fabricating BIO-133-sided substrates for chemically stimulating *C. elegans*. 1) Make PDMS channels and a 150 µm thick PDMS film. 2) Cut PDMS to desired size. Punch a 3.5 mm diameter hole in the film. Punch input and output ports to the PDMS channel. 3) Bond PDMS layers and glass with oxygen plasma treatment. 4) Cure a 80 µm thick BIO-133

film. 5) Immobilize worms in PEG-DA hydrogel. 6) Put the PEG-DA in the 3.5 mm hole contained within the PDMS film, cover the hole with BIO-133 and image.

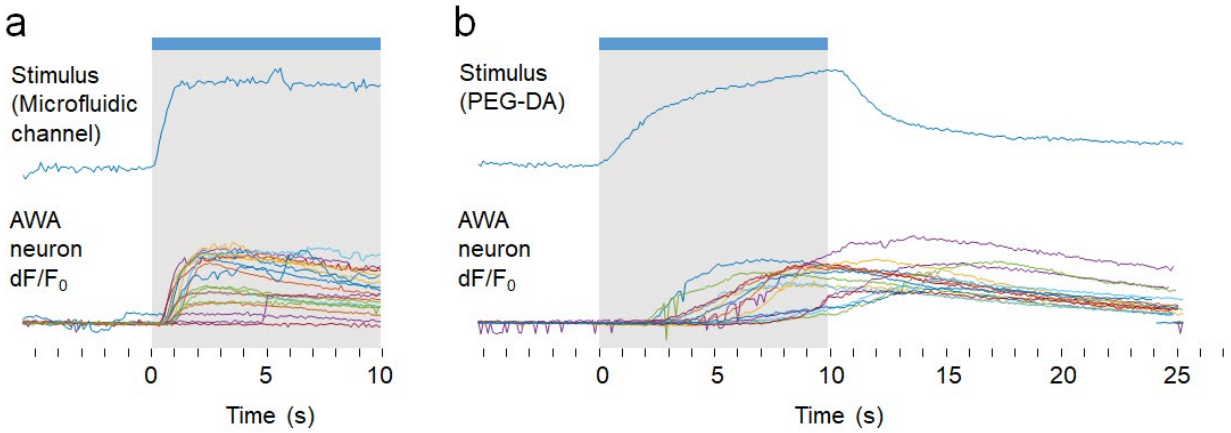

Supplementary Fig. 14, Diffusion of the chemical stimulus through the BIO-133/PEG-DA/PDMS device delays neural responses by a few seconds. a) In a microfluidic channel, stimulus (100 ng/mL fluorescein, 1.1 μm diacetyl) switch within 1 s and sensory neurons of animals in the channel respond with a 0.5-1 s delay. Mean fluorescence of fluorescein dye "stimulus" (above) and normalized AWA neuron fluorescence (below). Individual animal responses are shown by colors. b) Animals embedded in a PEG hydrogel disk above a microfluidic channel experience a slower stimulus onset and offset, and a corresponding delay in neural response, due to chemical diffusion into and out of the hydrogel.

Supplementary Table 1a, Apparent size of 100 nm yellow-green beads as imaged through different thicknesses of different polymers. Full width at half maximum (FWHM) for xyz dimensions as defined as in **Fig. 1c**. Note that defining 'z' this way leads to an underestimation of the FWHM along the direction of greatest elongation for the asymmetric images produced with PEG-DA, PDMS, and FEP. Means and standard deviations are shown; number of measurements is listed in parentheses after each x measurement.

FWHM-x(nm)				
Thickness(μm)	BIO-133	PEG-DA	PDMS	FEP
0	395.9±7.7 (70)	395.9±7.7 (70)	395.9±7.7 (70)	395.9±7.7 (70)
25	396.5±7.3 (68)	456.4±15.5 (53)	816.8±24.9 (48)	670.5±26.3 (53)
50	397.5±7.8 (60)	512.9±18.0 (42)	1005.5±64.3 (36)	734.6±40.4 (76)
75	403.8±8.5 (65)	622.9±22.0 (35)	1154.0±54.5 (69)	783.5±46.6 (65)
100	406.7±6.4 (70)	703.1±28.0 (23)	1235.6±72.4 (55)	
125	410.8±9.1 (68)	736.0±30.7 (42)	1302.2±56.9 (42)	1079.2±51.9 (71)
150	416.5±8.5 (57)	816.3±23.1 (38)	1383.8±53.2 (38)	
FWHM-y(nm)				
Thickness(μm)	BIO-133	PEG-DA	PDMS	FEP
0	400.8±7.6	400.8±7.6	400.8±7.6	400.8±7.6
25	395.2±7.5	399.5±6.5	433.9±12.6	398.8±9.3
50	402.5±10.9	410.7±9.0	450.8±20.3	441.0±12.1
75	399.9±9.5	422.7±13.4	460.9±22.1	478.2±18.1
100	396.1±8.7	424.7±14.3	483.8±20.5	
125	403.4±12.2	417.9±9.6	495.5±22.7	542.2±25.2
150	408.2±11.4	440.7±12.6	510.6±29.1	
FWHM-z(nm)				
Thickness(μm)	BIO-133	PEG-DA	PDMS	FEP
0	1527.9±119.5	1527.9±119.5	1527.9±119.5	1527.9±119.5
25	1527.8±120.5	1480.6±88.7	1535.4±140.7	1603.9±61.6
50	1544.9±133.6	1578.5±90.5	1550.6±81.1	1640.4±73.4
75	1497.8±110.3	1397.5±51.7	1678.2±102.4	1661.2±97.0
100	1542.1±126.5	1394.5±37.5	1850.1±96.1	
125	1505.9±114.2	1445.3±75.8	2018.7±127.3	1920.6±112.3
150	1436.9±65.6	1413.2±48.3	2008.3±134.2	

Supplementary Table 1b, **Apparent size of 100 nm yellow-green beads as imaged through different materials, using iSIM**. Full width at half maximum (FWHM) for xyz dimensions are shown (means +/- standard deviation), for raw and deconvolved data (5 iterations Richardson-Lucy deconvolution). Number of measurements is listed in parentheses after each x measurement. The asymmetry in x and y is due to a systematic astigmatism aberration in our setup. Beads in PDMS were imaged with 2.5x longer exposures as other measurements to obtain acceptable SNR. The 'Water' column refers to beads imaged directly on glass coverslips, all other measurements were performed through 50 μm of the indicated material.

.

	Water	**BIO-133**	**2% Agarose**	**PDMS**
Raw-x (nm)	250.6±12.0 (17)	256.5±12.1 (19)	267.2±9.9 (12)	293.9±18.8 (15)
Raw-y (nm)	194.2±9.1	192.0±14.3	210.7±10.9	243.1±9.6
Raw-z (nm)	635.3±23.5	643.5±28.8	820.6±38.9	1479.7±97.1
Decon-x (nm)	213.5±12.1 (17)	217.0±12.9 (19)	218.3±9.8 (12)	242.7±15.6 (15)
Decon-y (nm)	161.4±12.3	166.1±19.5	177.7±17.7	203.3±12.2
Decon-z (nm)	450.2±17.0	464.7±18.1	580.0±27.2	972.9±72.1

Supplementary Table 2a, Acquisition parameters for all cellular data acquired in this work. See also **Methods**. Here 'iSPIM' refers to single-view diSPIM.

Samples		**Live U2OS, mitochondrial label**			**Live WT HCT-116, lysosome label**	**Live HCT-116 TOP1-GFP**	**Fixed WT HCT-116, immunolabel**	**Fixed U2OS, DAPI**
Figures/Videos		Fig. 2 c, d Sup. Video 1	Fig. 2 f, g Sup. Video 3	Fig. 4 b, c Sup. Video 9	Sup. Fig. 7 Sup. Video 4	Sup. Fig. 3	Fig. 2 h, i Sup. Video 5	Sup. Fig. 6 Sup. Video 2
Fluorescence label		mEmerald-Tomm20			LAMP1-GFP	Topoisomerase I-GFP	Lamin A-JF549 Tomm20-AF488 Phalloidin AF647	DAPI
Microscope		diSPIM	iSIM	diSPIM	iSIM	iSIM	iSIM	diSPIM (iSPIM)
View number		2	1	2	1	1	1	1
Color number		1	1	1	1	1	3	1
Acquisition	Excitation, nm	488	488	488	488	488	488/561/633	405
	Step size x Slices per view per color	0.5 µm x 150 slices	0.25 µm x 8 slices	1 µm x 60 slices	0.5 µm x 26 slices	0.5 µm x 24 slices	0.5 µm x 46 slices	1 slice
	Acquisition time per time point	2.8 s	1 s	3 s	3 s	-	-	20 ms
	Time interval	3 s	3 s	60 s	7 s	-	-	20 ms
	Total time points	50	25	90	60	1	1	1000
	Total acquisition time	150 s	75 s	90 min	420 s	3 s	15 s	20 s
Data processing	Registration	√	x	√	x	x	x	x
	Deconvolution	√	√	√	√	√	√	x
	Bleach correction	√	√	√	√	x	488x/561x/633 √	x
	Drift correction	√	x	√	x	x	x	x

Supplementary Table 2b, Acquisition parameters for all tissue/animal data used in this work. See also **Methods**. Here 'iSPIM' refers to single-view diSPIM and 'PHD' to pleckstrin homology domain, localizing GFP to the cell surface.

Samples		**Live fly wing**	***C. elegans* neuron**	***C. elegans* neuron**		***C. elegans* AWA neuron**		
Figures/Videos		Fig. 3 b, c Sup. Video 6	Fig. 3 d	Fig. 3 e Sup. Video 7	Fig. 3 h Sup. Video 8	Fig. 4 e	Fig. 4 f Sup. Video 10	Fig. 4 h Sup. Video 11
Fluorescence label		CD4-tdTomato	PHD-GFP	GCaMP6s-pan-neuronal nuclei, tagRFP-pan-neuronal-nuclei		GCaMP2.2b		
Microscope		diSPIM (iSPIM)	diSPIM	diSPIM	diSPIM (iSPIM)	Widefield	diSPIM (iSPIM)	diSPIM (iSPIM)
View number		1	2	2	1	1	1	1
Color number		1	1	2	2	1	1	1
Acquisition	Excitation, nm	561	488	488/561	488/561	488	488	488
	Step size x Slices per view per color	1 µm x 70 slices	1 µm x 50 slices	1 µm x 40 slices	1 µm x 28 slices	1 slice	1.5 µm x 20 slices	1.5 µm x 30 slices
	Acquisition time per time point	3.8 s	-	0.7 s	245 ms	10 ms	0.56 s	0.68 s
	Time interval	5 s	-	0.8 s	0.25 s	100 ms	1 s	1s
	Total time points	360	1	450	250	300	45	600
	Total acquisition time	30 min	2.3 s	360 s	62.5 s	30 s	45 s	10 min
Data processing	Registration	x	√	√	x	x	x	x
	Deconvolution	√	√	√	√	x	x	x
	Bleach correction	√	x	x	x	x	x	x
	Drift correction	x	x	x	x	x	x	x

Supplementary Table 3, Mechanical properties of BIO-133 and PDMS. Data for BIO-133 is provided by the manufacturer, My Polymers.

	BIO-133 (My Polymers)	**PDMS (Dow Sylgard 184)**	**UV-PDMS (Shin-Etsu)**
Refractive index @589nm	**1.334**	**1.4118**	**1.407***
Elastic modulus (Young's modulus), MPa	5	1.3~3**	-
Tensile Strength, MPa	-	6.7	7.7
Elongation at Break, %	60	50-93**	110
Hardness, Shore A	70	43	55

*Self-measured

**Johnston, I D, D K McCluskey, C K L Tan, and M C Tracey. "Mechanical Characterization of Bulk Sylgard 184 for Microfluidics and Microengineering." *Journal of Micromechanics and Microengineering* 24, no. 3 (March 1, 2014): 035017. https://doi.org/10.1088/0960-1317/24/3/035017.